Improving Tumor-Targeting Capability and Pharmacokinetics of ^{99m}Tc-Labeled Cyclic RGD Dimers with PEG$_4$ Linkers

Lijun Wang[1], **Jiyun Shi**[1], **Young-Seung Kim**[1], **Shizhen Zhai**[1], **Bing Jia**[2], **Huiyun Zhao**[2], **Zhaofei Liu**[3], **Fan Wang**[2], **Xiaoyuan Chen**[3], and **Shuang Liu**[1],*

1 *School of Health Sciences, Purdue University, IN 47907, USA*

2 *Medical Isotopes Research Center, Peking University, Beijing 100083, China*

3 *Molecular Imaging Program at Stanford, Department of Radiology & Bio-X, Stanford University, Stanford, California, USA*

Abstract

This report describes the synthesis of two cyclic RGD (Arg-Gly-Asp) conjugates, HYNIC-2PEG$_4$-dimer (HYNIC = 6-hydrazinonicotinyl; 2PEG$_4$-dimer = E[PEG$_4$-c(RGDfK)]$_2$; and PEG$_4$ = 15-amino-4,7,10,13-tetraoxapentadecanoic acid) and HYNIC-3PEG$_4$-dimer (3PEG$_4$-dimer = PEG$_4$-E[PEG$_4$-c(RGDfK)]$_2$), and evaluation of their ^{99m}Tc complexes [^{99m}Tc(HYNIC-2PEG$_4$-dimer)(tricine)(TPPTS)] (^{99m}Tc-2PEG$_4$-dimer: TPPTS = trisodium triphenylphosphine-3,3′,3″-trisulfonate) and [^{99m}Tc(HYNIC-3PEG$_4$-dimer)(tricine)(TPPTS)] (^{99m}Tc-3PEG$_4$-dimer) as novel radiotracers for imaging integrin $\alpha_v\beta_3$ expression in athymic nude mice bearing U87MG glioma and MDA-MB-435 breast cancer xenografts. The integrin $\alpha_v\beta_3$ binding affinities of RGD peptides were determined by competitive displacement of ^{125}I-c(RGDyK) on U87MG glioma cells. It was found that the two PEG$_4$ linkers between RGD motifs in HYNIC-2PEG$_4$-dimer (IC$_{50}$ = 2.8 ± 0.5 nM) and HYNIC-3PEG$_4$-dimer (IC$_{50}$ = 2.4 ± 0.7 nM) are responsible for their higher integrin $\alpha_v\beta_3$ binding affinity than that of HYNIC-PEG$_4$-dimer (PEG$_4$-dimer = PEG$_4$-E[c(RGDfK)]$_2$; IC$_{50}$ = 7.5 ± 2.3 nM). Addition of extra PEG$_4$ linker in HYNIC-3PEG$_4$-dimer has little impact on integrin $\alpha_v\beta_3$ binding affinity. ^{99m}Tc-2PEG$_4$-dimer and ^{99m}Tc-3PEG$_4$-dimer were prepared in high yield with >95% radiochemical purity and the specific activity of > 10 Ci/µmol. Biodistribution studies clearly demonstrated that PEG$_4$ linkers are particularly useful for improving the tumor uptake and clearance kinetics of ^{99m}Tc-2PEG$_4$-dimer and ^{99m}Tc-3PEG$_4$-dimer from non-cancerous organs. It was also found that there was a linear relationship between the tumor size and radiotracer tumor uptake expressed as %ID (percentage of the injected dose) in U87MG glioma and MDA-MB-435 breast tumor models. The blocking experiment showed that the tumor uptake of ^{99m}Tc-2PEG$_4$-dimer is integrin $\alpha_v\beta_3$-mediated. In the metabolism study, ^{99m}Tc-2PEG$_4$-dimer had high metabolic stability during its excretion from renal and hepatobiliary routes. ^{99m}Tc-3PEG$_4$-dimer also remained intact during thee excretion from the renal route, but, had ~30% metabolism during the excretion from the hepatobiliary route. Planar imaging studies in U87MG glioma and MDA-MB-435 breast tumor models showed that the tumors of ~5 mm in diameter could be readily visualized with excellent contrast. Thus, ^{99m}Tc-3PEG$_4$-dimer is a very promising radiotracer for the early detection of integrin $\alpha_v\beta_3$–positive tumors, and may have the potential for non-invasive monitoring of tumor growth or treatment efficacy.

*To whom correspondence should be addressed: School of Health Sciences, Purdue University, 550 Stadium Mall Drive, West Lafayette, IN 47907. Phone: 765-494-0236; Fax 765-496-1377; Email: lius@pharmacy.purdue.edu.

Keywords

integrin $\alpha_v\beta_3$; [99mTc]-labeled peptides; cyclic RGD dimers; tumor imaging

INTRODUCTION

Integrin $\alpha_v\beta_3$ plays a critical role in tumor angiogenesis and metastasis.[1–8] The highly restricted expression of integrin $\alpha_v\beta_3$ during tumor growth, invasion and metastasis makes it an interesting molecular target for the development of integrin $\alpha_v\beta_3$-targeted therapeutic drugs and molecular imaging probes.[9–18] Many high affinity cyclic RGD (Arg-Gly-Asp) peptides and non-peptide integrin $\alpha_v\beta_3$ antagonists have been identified and studied for their potential as therapeutic pharmaceuticals for the treatment of solid tumors.[13–18] These anti-angiogenic agents were designed to block the formation of new blood vessels and destroy existing abnormal blood vessels by starving tumors and inhibiting their growth. They have also been shown to increase therapeutic efficacy in conjunction with other therapeutic agents or with external radiotherapy.[19] Inhibition of integrin $\alpha_v\beta_3$ by cyclic RGD peptides has been shown to induce endothelial apoptosis,[15] inhibit angiogenesis,[17] and increase endothelial monolayer permeability.[19, 20] The inhibition of integrin $\alpha_v\beta_3$ activity has been associated with the decreased tumor growth in breast cancer xenografts.[19] Synergy of the cyclic RGD peptide EMD 121974 with radioimmunotherapy (RIT) increased the efficacy of therapy in a murine breast cancer model.[19] However, there are several significant challenges for successful anti-angiogenic clinical trials: (1) selection of the right patients who will benefit the most, given that only the integrin $\alpha_v\beta_3$–positive patients are responsive to the specific anti-angiogenic treatment; (2) monitoring the therapeutic efficacy of the anti-angiogenic treatment; and (3) individualizing the optimal dose and schedule of anti-angiogenic treatment for specific patients. To achieve these goals, it is essential to develop an imaging agent that could be used for non-invasive visualization and quantification of the integrin $\alpha_v\beta_3$ expression level before and during the anti-angiogenic therapy.

Over the last decade, many radiolabeled cyclic RGD peptides have been evaluated as potential radiotracers for noninvasive imaging of integrin $\alpha_v\beta_3$-positive tumors by single photon emission computed tomography (SPECT) or positron emission tomography (PET).[20–36] The integrin $\alpha_v\beta_3$-targeted radiotracers have recently been reviewed extensively.[37–43] Among these radiotracers evaluated in different tumor-bearing animal models, [[18F]]Galacto-RGD (2-[[18F]fluoropropanamide-c(RGDfK(SAA); SAA = 7-amino-L-glyero-L-galacto-2,6-anhydro-7-deoxyheptanamide) and [[18F]]-AH111585, the core peptide sequence of which was originally discovered from a phage display library (as ACDRGDCFCG),[44] are currently under clinical investigation for noninvasive visualization of integrin $\alpha_v\beta_3$ expression.[44–46] The PET imaging studies in cancer patients clearly show that the integrin $\alpha_v\beta_3$ expression level correlates well with radiotracer tumor uptake.[44–46] Although they are able to target integrin $\alpha_v\beta_3$-positive tumors, the relatively low tumor uptake, suboptimal pharmacokinetics, high cost and lack of preparative modules for the [18F]-labeled monomeric RGD peptides are significant challenges for their continued clinical applications.

Since the natural mode of interactions between integrin $\alpha_v\beta_3$ and the RGD-containing proteins, such as fibronectin and vitronectin, may involve multiple binding sites, the idea to improve integrin $\alpha_v\beta_3$ affinity with multimeric cyclic RGD peptides may provide more effective integrin $\alpha_v\beta_3$ antagonists with better targeting capability and higher cellular uptake through the integrin-dependent endocytosis.[47] Multivalent interactions are designed to make weak ligand-receptor interactions more biologically relevant.[48] Over the last several years, we and others have been using multimeric cyclic RGD peptides, such as E[c(RGDxK)]$_2$ and E{E[c(RGDxK)]$_2$}$_2$ (x = f (D-Phe) and y (D-Tyr)), to develop the integrin $\alpha_v\beta_3$-targeted radiotracers for imaging tumors

by SPECT or PET.[49–62] In general, there are two main factors (Figure 1: simultaneous integrin $\alpha_v\beta_3$ binding of two RGD motifs and the locally enriched RGD concentration) that contribute to the higher integrin $\alpha_v\beta_3$ binding affinity of E[c(RGDfK)]$_2$ and E{E[c(RGDfK)]$_2$}$_2$ than that of their monomeric counterpart c(RGDfK). The key for "bivalency" is that the distance between two RGD motifs in multimeric cyclic RGD peptides must be long enough and flexible enough to achieve simultaneous integrin $\alpha_v\beta_3$ binding. If the distance between two cyclic RGD motifs is long enough, the multimeric cyclic RGD peptides would bind to the integrin $\alpha_v\beta_3$ in a "bidentate" fashion (Figure 1A). If the distance between two cyclic RGD motifs in multimeric cyclic RGD peptides is too short to achieve simultaneous integrin $\alpha_v\beta_3$ binding, the local RGD concentration would be significantly "enriched" in the vicinity of the neighboring integrin $\alpha_v\beta_3$ sites once the first RGD motif is bound to integrin $\alpha_v\beta_3$ (Figure 1B). In both cases, increasing the multiplicity would result in higher integrin $\alpha_v\beta_3$ binding affinity of multimeric cyclic RGD peptides and better tumor uptake with longer tumor retention time for their corresponding radiotracers. Although in vitro assays and ex-vivo biodistribution studies have demonstrated that the radiolabeled (^{99m}Tc, ^{18}F, ^{64}Cu and ^{111}In) multimeric cyclic RGD peptides, such as E{E[c(RGDxK)]$_2$}$_2$ and E[c(RGDxK)]$_2$ (x = f and y), have much better tumor targeting capability as evidenced by their higher integrin $\alpha_v\beta_3$ binding affinity and better radiotracer tumor uptake than their monomeric analogs,[51–62] it remains unclear if the cyclic RGD motifs in E[c(RGDfK)]$_2$ and E{E[c(RGDfK)]$_2$}$_2$ are able to achieve simultaneous integrin $\alpha_v\beta_3$ binding. In addition, the uptake of the radiolabeled (^{99m}Tc, ^{18}F, ^{64}Cu and ^{111}In) multimeric cyclic RGD peptides in the kidneys, liver, lungs and spleen is also significantly increased as the peptide multiplicity increases.

To solve these problems, we prepared a new cyclic RGD peptide dimer: E[PEG$_4$-c(RGDfK)]$_2$ (Figure 2: 2PEG$_4$-dimer, PEG$_4$ = 15-amino-4,7,10,13-tetraoxapentadecanoic acid). Two PEG$_4$ linkers were used to increase the distance between two RGD motifs from 6 bonds in E[c(RGDfK)]$_2$ to 38 bonds in 2PEG$_4$-dimer excluding side arms of K-residues. We also prepared PEG$_4$-E[PEG$_4$-c(RGDfK)]$_2$ (Figure 2: 3PEG$_4$-dimer), in which an extra PEG$_4$ was added to improve radiotracer excretion kinetics from non-cancerous organs, such as kidneys, liver and lungs. We are particularly interested in ^{99m}Tc due to its optimal nuclear characteristics (half-life, abundance and energy of γ-photons) and easy availability at low cost.[11,63–65] For ^{99m}Tc-labeling, 6-hydrazinonicotinyl (HYNIC) was used as the bifunctional coupling agent whereas tricine and TPPTS (trisodium triphenylphosphine-3,3′,3″-trisulfonate) were used to stabilize the ^{99m}Tc-HYNIC core in ^{99m}Tc complexes: [^{99m}Tc(HYNIC-2PEG$_4$-dimer)(tricine)(TPPTS)] (^{99m}Tc-2PEG$_4$-dimer) and [^{99m}Tc(HYNIC-3PEG$_4$-dimer)(tricine)(TPPTS)] (^{99m}Tc-3PEG$_4$-dimer). An in vitro competition assay was used to determine the integrin $\alpha_v\beta_3$ binding affinity of HYNIC-2PEG$_4$-dimer and HYNIC-3PEG$_4$-dimer against ^{125}I-c(RGDyK) bound to the integrin $\alpha_v\beta_3$-positive U87MG human glioma cells. Biodistribution characteristics of ^{99m}Tc-2PEG$_4$-dimer and ^{99m}Tc-3PEG$_4$-dimer were evaluated in athymic nude mice bearing U87MG glioma and MDA-MB-435 breast cancer xenografts. For comparison purposes, we also evaluated HYNIC-PEG$_4$-c(RGDfK) (HYNIC-PEG$_4$-monomer), HYNIC-PEG$_4$-E[c(RGDfK)]$_2$ (HYNIC-PEG$_4$-dimer) and their ^{99m}Tc complexes, [^{99m}Tc(HYNIC-PEG$_4$-monomer)(tricine)(TPPTS)] (^{99m}Tc-PEG$_4$-monomer) and [^{99m}Tc(HYNIC-PEG$_4$-dimer)(tricine)(TPPTS)] (^{99m}Tc-PEG$_4$-dimer). The main objective of this study is to demonstrate that the use of PEG$_4$ linkers will make it possible for the two cyclic RGD motifs in ^{99m}Tc-2PEG$_4$-dimer and ^{99m}Tc-3PEG$_4$-dimer to achieve simultaneous integrin $\alpha_v\beta_3$ binding, thereby leading to higher integrin $\alpha_v\beta_3$ binding affinity for the cyclic RGD peptide dimer and better tumor uptake with longer tumor retention times for the corresponding ^{99m}Tc radiotracer. In addition, the presence of PEG$_4$ linkers should improve the radiotracer excretion kinetics from kidneys, liver and lungs. Improving the radiotracer tumor uptake and its excretion kinetics from non-cancerous organs is critically important for the early detection of integrin $\alpha_v\beta_3$–positive tumors.

EXPERIMENTAL SECTION

Materials

Dicyclcohexylcarbodiimide (DCC), N-hydroxysuccinimide (NHS), succinic acid, trisodium triphenylphosphine-3,3′,3″-trisulfonate (TPPTS) and tricine were purchased from *Sigma-Aldrich* (St. Louis, MO). Cyclic RGD peptide dimers, 2PEG$_4$-dimer and 3PEG$_4$-dimer were custom-made by Peptide International, Inc. (Louisville, KY). PEG$_4$-E[c(RGDfK)]$_2$ (PEG$_4$-dimer) was prepared according to the procedure described in our previous reports.[52] Sodium succinimidyl 6-(2-(2-sulfonatobenzaldehyde)hydrazono)nicotinate (HYNIC-NHS) was prepared according to literature method.[66] Na^{99m}TcO$_4$ was obtained from a commercial DuPont Pharma ^{99}Mo/^{99m}Tc generator (North Billerica, MA). The ESI (electrospray ionization) mass spectral data were collected on a Finnigan LCQ classic mass spectrometer, School of Pharmacy, Purdue University.

HPLC Methods

HPLC Method 1 used a LabAlliance HPLC system (State College, PA) equipped with a UV/Vis detector (λ = 254 nm) and Zorbax C$_{18}$ semi-prep column (9.4 mm $\times$ 250 mm, 100 Å pore size). The flow rate was 2.5 mL/min. The gradient mobile phase started with 90% solvent A (25 mM NH$_4$OAc) and 10% solvent B (acetonitrile) to 85% solvent A and 15% solvent B at 5 min to 65% solvent A and 35% solvent B at 30 min, followed by an isocratic mobile phase with 50% solvent A and 50% solvent B at 32 – 36 min. The radio-HPLC method (Method 2) used the LabAlliance HPLC system equipped with a β-ram IN/US detector (IN/US System, Tampa, FL) and Zorbax C$_{18}$ column (4.6 mm $\times$ 250 mm, 300 Å pore size; Agilent Technologies, Santa Clara, CA). The flow rate was 1 mL/min. The mobile phase was isocratic with 90% solvent A (25 mM NH$_4$OAc, pH = 5.0) and 10% solvent B (acetonitrile) at 0 – 2 min, followed by a gradient mobile phase going from 10% B at 2 min to 15% B at 5 min and to 20% solvent B at 20 min.

HYNIC-E[PEG$_4$-c(RGDfK)]$_2$ (HYNIC-2PEG$_4$-dimer)

HYNIC-NHS (4.6 mg, 11 µmol) and E[PEG$_4$-c(RGDfK)]$_2$ (5 mg, 2.8 µmol) were dissolved in 2.0 mL of a mixture containing DMF and water (50:50 = v:v). The pH in the mixture was adjusted to 8.5 – 9.0 using 0.1 N NaOH. The reaction mixture was then stirred overnight at room temperature. The product was isolated from the reaction mixture by HPLC purification (Method 1). The fraction at 19.6 min was collected. Lyophilization of the collected fractions afforded HYNIC-2PEG$_4$-dimer as a white powder. The yield was 2.0 mg (~34%) with >95% HPLC purity. ESI-MS (positive mode): m/z = 1058.59 for [M + 2H]$^{2+}$ (m/z = 1058.99 calcd. for [C$_{94}$H$_{140}$N$_{24}$O$_{30}$S]$^{2+}$).

HYNIC-PEG$_4$-E[PEG$_4$-c(RGDfk)]$_2$ (HYNIC-3PEG$_4$-dimer)

HYNIC-NHS (2 mg, 4.8 µmol) and 3PEG$_4$-dimer (2.4 mg, 1.2 µmol) were dissolved in a mixture (2 mL) of DMF and water (1:1 = v:v). The pH was adjusted to 8.5 – 9.0 with 0.1 N NaOH. The mixture was stirred overnight at room temperature. The product was isolated by HPLC purification (Method 1). Fractions at 20.6 min were collected. Lyophilization of the combined collections afforded the expected product HYNIC-3PEG$_4$-dimer. The yield was 1 mg (~35%) with >95% HPLC purity. ESI-MS: m/z = 2364.33 for [M+H]$^+$ (2364.1 calcd. For [C$_{105}$H$_{160}$N$_{25}$O$_{35}$S]$^+$).

HYNIC-PEG$_4$-c(RGDfK) (HYNIC-PEG$_4$-Monomer)

HYNIC-PEG$_4$-monomer was prepared using the same procedure using HYNIC-NHS (4.4 mg, 10.6 µmol) and PEG$_4$-c(RGDfk) (3 mg, 3.53 µmol). Lyophilization of the combined collections ~19.5 min (Method 1) afforded the expected product HYNIC-PEG$_4$-Monomer. The yield was

1.6 mg (~40%) with HPLC purity >95%. ESI-MS: $m/z = 1154.17$ for $[M+H]^+$ (1154.49 calcd. For $[C_{51}H_{72}N_{13}O_{16}S]^+$)

99mTc-Labeling

To a lyophilized vial containing 5 mg of TPPTS, 6.5 mg of tricine, 38.5 mg of disodium succinate hexahydrate, and 12.7 mg of succinic acid, 20 µg of the HYNIC-RGD conjugate (RGD = PEG$_4$-monomer, 2PEG$_4$-dimer or 3PEG$_4$-dimer) was added 1.0 – 1.5 mL of Na^{99m}TcO$_4$ solution (10 – 50 mCi) in saline. The vial was heated at 100 °C for 20 – 25 min in a lead-shielded water bath. After heating, the vial was placed back into the lead pig, and allowed to stand at room temperature for ~10 min. A sample of the resulting solution was analyzed by the radio-HPLC. The radiochemical purity (RCP) was >95% for all new ^{99m}Tc radiotracers.

Dose Preparation for Animal Studies

For biodistribution studies, all new radiotracers were prepared and then purified by HPLC (Method 2). Volatiles in the HPLC mobile phase were removed under vacuum. Doses were prepared by dissolving the HPLC-purified radiotracer in saline to 20 – 30 µCi/mL. For imaging studies, doses were prepared by dissolving the radiotracer in saline to 5 – 10 mCi/mL. In the blocking experiment, E[c(RGDfK)]$_2$ was dissolved in the solution containing the radiotracer to give a concentration of 1.75 mg/mL. The resulting solution was filtered with a 0.20 µ syringe-driven Millex-LG filter before being injected into animals. Each tumor-bearing mouse was injected with ~0.2 mL of the filtered dose solution.

Determination of Log P Values

The radiotracer was prepared and then purified by HPLC (Method 2). Volatiles in the HPLC mobile phase were removed under vacuum. The residue was dissolved in an equal volume (3 mL:3 mL) mixture of n-octanol and 25 mM phosphate buffer (pH = 7.4). After stirring vigorously for ~20 min, the mixture was centrifuged at a speed of 8,000 rpm for 5 min. Samples (in triplets) from both n-octanol and aqueous layers were obtained and counted in a Perkin Elmer Wizard – 1480 γ-counter (Shelton, CT). Partition coefficients were measured three different times. The log P values were reported as the average of three independent measurements plus the standard deviation.

In Vitro Whole-Cell Integrin α$_v$β$_3$ Binding Assay

The in vitro integrin binding affinity and specificity of multimeric cyclic RGD peptides were determined via a competitive displacement assay using ^{125}I-c(RGDyK) as the integrin-specific radioligand. Experiments were performed using the integrin α$_v$β$_3$-positive U87MG human glioma cell line by slight modification of the literature method.[39] For comparison purposes, we also evaluated c(RGDyK) using the same in vitro assay. Briefly, the U87MG glioma cells were grown in Gibco's Dulbecco's medium supplemented with 10% fetal bovine serum (FBS), 100 IU/mL penicillin and 100 µg/mL streptomycin (Invitrogen Co, Carlsbad, CA) at 37 °C in a humidified atmosphere containing 5% CO$_2$. Multiscreen DV filter plates were seeded with ~105 cells in the binding buffer and incubated with ^{125}I-c(RGDyK) in the presence of increasing concentrations of different cyclic RGD peptides or their HYNIC conjugates. After removing the unbound ^{125}I-c(RGDyK), hydrophilic PVDF filters were collected and the radioactivity was determined using a gamma counter (Packard, Meriden, CT). The IC$_{50}$ values were calculated by fitting the data by nonlinear regression using GraphPad Prism™ (GraphPad Software, Inc., San Diego, CA). All the in vitro experiments were carried out twice with triplicate samples. The IC$_{50}$ values were calculated, and reported as an average of these samples plus the standard deviation. Comparison between two different cyclic RGD peptides was made

using the two-way ANOVA test (GraphPad Prim 5.0, San Diego, CA). The level of significance was set at $p < 0.05$.

Animal Model

Biodistribution and imaging studies were carried out using the athymic nude mice bearing U87MG human glioma and MDA-MB-435 human breast cancer xenografts in compliance with the NIH animal experiment guidelines (*Principles of Laboratory Animal Care*, NIH Publication No. 86-23, revised 1985). The animal protocol for these studies has been approved by the Purdue University Animal Care and Use Committee (PACUC). U87MG glioma and MDA-MB-435 breast cancer cells were grown at 37 °C in Minimal Essential Medium (Alpha Modification) containing 3.7 g of sodium bicarbonate/L, 10% fetal bovine serum v/v, in a humidified atmosphere of 5% carbon dioxide. Female athymic nu/nu mice were purchased from Harlan (Indianapolis, IN) at 4 – 5 weeks of age. Each mouse was implanted subcutaneously with 5×10^6 tumor cells into the left and right upper flanks (for the glioma model) or the left and right mammary fat pads (for the breast cancer model). Doing so allows us to assess the impact of tumor size on the radiotracer imaging quality in a single tumor-bearing mouse. Two to four weeks after inoculation, animals with tumors in the range of 0.05 – 1.7 g were used for biodistribution and imaging studies.

Biodistribution Protocol

Twelve tumor-bearing mice with the tumor size of 0.05 – 0.4 g were randomly divided into three groups. The ^{99m}Tc radiotracer (~2 μCi) in 0.1 mL saline was administered via tail vein. Four animals were sacrificed by sodium pentobarbital overdose (100 mg/kg) at 30, 60, and 120 min postinjection (p.i.). Blood samples were withdrawn from the heart. The tumor and normal organs (brain, eyes, spleen, lungs, liver, kidneys, muscle and intestine) were excised, washed with saline, dried with absorbent tissue, weighed, and counted on a Perkin Elmer Wizard – 1480 γ-counter (Shelton, CT). The organ uptake was calculated as a percentage of the injected dose per organ (%ID/organ) and a percentage of the injected dose per gram of organ tissue (% ID/g). For the blocking experiment, each animal was administered with ~2 μCi of ^{99m}Tc-2PEG$_4$-dimer along with ~350 μg of E[c(RGDfK)]$_2$ (~14 mg/kg). At 1 h p.i., four animals were sacrificed by sodium pentobarbital overdose (100 mg/kg) for organ biodistribution. The organ uptake (%ID/g) was compared to that obtained in the absence of excess E[c(RGDfK)]$_2$ at the same time point.

Scintigraphic Imaging

Two tumor-bearing mice bearing U87MG glioma or MDA-MB-435 breast cancer xenografts were used for imaging studies with ^{99m}Tc-3PEG$_4$-dimer. The tumor-bearing mice were anesthetized with intraperitoneal injection of Ketamine (40 – 100 mg/kg) and Xylazine (2 – 5 mg/kg). Each animal was administered with 0.5 – 1.0 mCi of ^{99m}Tc-3PEG$_4$-dimer. Animals were placed prone on a single head mini γ-camera (Diagnostic Services Inc., NJ) equipped with a parallel-hole, low-energy, and high-resolution collimator. Static images were acquired at 30, 60, 120 and 240 min p.i. and stored digitally in a 128×128 matrix. The acquisition count limits were set at 500 K. For the blocking experiment with ^{99m}Tc-3PEG$_4$-dimer in the U87MG glioma model, the same procedure was used except that E[c(RGDfK)]$_2$ (~14 mg/kg or ~350 μg per mouse) was co-injected as the blocking agent. After imaging, the mice were euthanized by sodium pentobarbital overdose (100 – 200 mg/kg).

Metabolism

Two normal athymic nude mice were used for the metabolism study of each ^{99m}Tc radiotracer. Each mouse was administered with 100 – 120 μCi of the ^{99m}Tc radiotracer via tail vein. The urine samples were collected at 30 min and 120 min p.i. by manual void, and were mixed with

equal volume of 20% acetonitrile aqueous solution. The mixture was centrifuged at 8,000 rpm. The supernatant was collected and filtered through a 0.20 µ Millex-LG syringe-driven filter unit. The filtrate was analyzed by radio-HPLC (Method 2). The feces samples were collected at 2 h p.i. and suspended in the 20% acetonitrile aqueous solution (2 mL). The resulting mixture was vortexed for 5 – 10 min. After centrifuging at 8,000 rpm for 5 min, the supernatant was collected and passed through a 0.20 µ Millex-LG syringe-driven filter unit to remove any precipitate or particles. The filtrate was analyzed by radio-HPLC (Method 2).

Data and Statistical Analysis

The biodistribution data and target-to-background (T/B) ratios are reported as an average plus the standard variation based on results from four tumor-bearing mice at each time point. Comparison between two different ^{99m}Tc radiotracers was made using the two-way ANOVA test (GraphPad Prim 5.0, San Diego, CA). The level of significance was set at $p < 0.05$.

RESULTS

HYNIC-RGD Conjugate Synthesis

Cyclic RGD peptide conjugates, HYNIC-PEG$_4$-monomer, HYNIC-2PEG$_4$-dimer and HYNIC-3PEG$_4$-dimer were prepared by conjugation of PEG$_4$-monomer, 2PEG$_4$-dimer and 3PEG$_4$-dimer, respectively, with excess HYNIC-NHS in DMF. All new HYNIC conjugates were purified by HPLC (Method 1) and characterized by ESI-MS. The ESI-MS data were completely consistent with their proposed formula. Their HPLC purity of HYNIC conjugates was >95% before being used for ^{99m}Tc-labeling and determination of their integrin $\alpha_v\beta_3$ binding affinity.

Integrin $\alpha_v\beta_3$ Binding Affinity

We determined the integrin $\alpha_v\beta_3$ binding affinity of HYNIC-PEG$_4$-monomer, HYNIC-2PEG$_4$-dimer and HYNIC-3PEG$_4$-dimer by displacement of ^{125}I-c(RGDyK) bound to U87MG human glioma cells. For comparison purposes, we also evaluated c(RGDyK), HYNIC-PEG$_4$-dimer and HYNIC-tetramer in the same assay. IC$_{50}$ values were calculated to be 37.3 ± 10.1, 31.7 ± 9.7, 7.5 ± 2.3, 2.9 ± 0.7, 2.4 ± 0.7 and 2.8 ± 0.5 nM for c(RGDyK), HYNIC-PEG$_4$-monomer, HYNIC-PEG$_4$-dimer, HYNIC-2PEG$_4$-dimer, HYNIC-3PEG$_4$-dimer and HYNIC-tetramer, respectively.

Radiochemistry

All three new radiotracers (^{99m}Tc-PEG$_4$-monomer, ^{99m}Tc-2PEG$_4$-dimer and ^{99m}Tc-3PEG$_4$-dimer) were prepared in high yield (>95%) using the non-SnCl$_2$ formulation.[21,31,67] The specific activity was >5 mCi/µg (or 10 Ci/µmol of a ~2000 Dalton HYNIC-RGD conjugate) for both ^{99m}Tc-2PEG$_4$-dimer and ^{99m}Tc-3PEG$_4$-dimer. All three radiotracers were stable in the kit matrix for >6 h, which is consistent with the results from our previous studies.[31,68–70] The HPLC retention times of ^{99m}Tc-PEG$_4$-monomer, ^{99m}Tc-2PEG$_4$-dimer and ^{99m}Tc-3PEG$_4$-dimer are listed in Table 1. We also determined their partition coefficients (P values) in an equal volume mixture of n-octanol and 25 mM phosphate buffer (pH = 7.4). The log P values for ^{99m}Tc-PEG$_4$-monomer, ^{99m}Tc-2PEG$_4$-dimer and ^{99m}Tc-3PEG$_4$-dimer were calculated to be −4.23 ± 0.21, −4.04 ± 0.15 and −3.96 ± 0.05, respectively. These values were slightly lower than that reported for ^{99m}Tc-PEG$_4$-dimer (log P = −3.56 ± 0.16).[60]

It is interesting to note that ^{99m}Tc-PEG$_4$-monomer, ^{99m}Tc-2PEG$_4$-dimer and ^{99m}Tc-3PEG$_4$-dimer all showed a single radiometric peak in their radio-HPLC chromatograms using the chromatographic conditions described in this study. In ternary ligand complexes [^{99m}Tc(HYNIC-BM)(tricine)(TPPTS)] (BM = targeting biomolecule), the Tc chelate is chiral because

the tricine coligand is "prochiral". As a result, complexes [^{99m}Tc(HYNIC-BM)(tricine) (TPPTS)] are often formed as a 50%:50% mixture of two diastereomers if BM has one or more chiral centers in its backbone.[65,68,70] Attempts to separate these two diastereomers in ^{99m}Tc-PEG$_4$-monomer, ^{99m}Tc-2PEG$_4$-dimer and ^{99m}Tc-3PEG$_4$-dimer by using different reversed-phase HPLC columns, buffering agents, mobile phase gradients and flow rates were not successful. Apparently, the presence of PEG$_4$ groups made separation of these two diastereomers much more difficult.

Biodistribution Characteristics in Breast Cancer Model

The athymic nude mice bearing MDA-MB-435 human breast cancer xenografts were used to study the biodistribution characteristics and excretion kinetics of ^{99m}Tc-2PEG$_4$-dimer. For comparison purposes, we evaluated ^{99m}Tc-PEG$_4$-dimer in the same animal model with very similar tumor size (0.1 – 0.5 g). Figure 4 compares the %ID/g tumor uptake and selected T/B ratios of ^{99m}Tc-PEG$_4$-dimer, ^{99m}Tc-2PEG$_4$-dimer and ^{99m}Tc-tetramer. Detailed biodistribution data for ^{99m}Tc-2PEG$_4$-dimer and ^{99m}Tc-PEG$_4$-dimer are listed in Tables SI and SII, respectively. The biodistribution data and T/B ratios of ^{99m}Tc-tetramer in the same tumor-bearing animal model were obtained from our previous report.[53]

The tumor uptake of ^{99m}Tc-2PEG$_4$-dimer was 5.20 ± 1.74 %ID/g at 30 min p.i. and 9.77 ± 2.66 %ID/g at 120 min p.i., which was well comparable to that of ^{99m}Tc-tetramer (5.78 ± 0.67 %ID/g at 30 min p.i. and 7.30 ± 1.32 %ID/g at 120 min p.i.) within the experimental error. In contrast, the tumor uptake of ^{99m}Tc-PEG$_4$-dimer was only 3.49 ± 0.62 %ID/g at 30 min p.i. and 3.82 ± 0.54 %ID/g at 120 min p.i. in the same model. ^{99m}Tc-2PEG$_4$-dimer had a liver uptake of 2.97 ± 0.63 %ID/g at 30 min p.i. and 3.27 ± 1.09 %ID/g at 120 min p.i. The liver uptake of ^{99m}Tc-tetramer was 4.76 ± 0.72 %ID/g at 30 min p.i., and 4.09 ± 0.59 %ID/g at 120 min p.i.[53] The kidney uptake of ^{99m}Tc-2PEG$_4$-dimer (14.37 ± 4.09 %ID/g and 13.78 ± 5.36 % ID/g at 30 and 120 min p.i., respectively) was only half of that for ^{99m}Tc-tetramer (32.84 ± 4.27 %ID/g at 30 min p.i. and 25.93 ± 2.52 %ID/g at 120 min p.i.). The muscle uptake of ^{99m}Tc-2PEG$_4$-dimer (1.76 ± 0.56 %ID/g at 30 min p.i. and 1.51 ± 0.35 %ID/g at 120 min p.i.) was slightly lower than that of ^{99m}Tc-tetramer (2.41 ± 0.54 %ID/g at 30 min p.i. and 2.09 ± 0.70 %ID/g at 120 min p.i.).[53] The tumor/muscle ratio of ^{99m}Tc-2PEG$_4$-dimer was 6.52 ± 1.72 at 120 min, which was much better ($p < 0.01$) than that of ^{99m}Tc-PEG$_4$-dimer (2.91 ± 0.60 at 120 min).

Blocking Experiment

In this experiment, ^{99m}Tc-2PEG$_4$-dimer was used as radiotracer and E[c(RGDfK)]$_2$ as the blocking agent (~14 mg/kg or ~350 μg per tumor-bearing mouse). Figure 5 compares the organ uptake of ^{99m}Tc-2PEG$_4$-dimer at 60 min p.i. in the absence or presence of excess E[c (RGDfK)]$_2$. Co-injection of excess E[c(RGDfK)]$_2$ resulted in dramatic reduction in the tumor uptake of ^{99m}Tc-2PEG$_4$-dimer (2.43 ± 0.07 %ID/g with E[c(RGDfK)]$_2$ vs. 8.30 ± 3.57 %ID/g without E[c(RGDfK)]$_2$). There was also a significant reduction of its uptake in the eyes, heart, intestine, lungs, liver and spleen (Figure 5), however, its uptake in the blood and kidneys in the presence of E[c(RGDfK)]$_2$ was comparable to that obtained without E[c(RGDfK)]$_2$.

Biodistribution Characteristics in Glioma Model

To further confirm our findings in the MDA-MB-435 breast cancer model, we also evaluated the tumor uptake and biodistribution properties of ^{99m}Tc-PEG$_4$-monomer, ^{99m}Tc-2PEG$_4$-dimer and ^{99m}Tc-3PEG$_4$-dimer in athymic nude mice bearing U87MG glioma xenografts. The tumor size was very close (0.1 – 0.5 g) in these two tumor-bearing animal models. These studies were designed to: (1) demonstrate the superiority of ^{99m}Tc-2PEG$_4$-dimer and ^{99m}Tc-3PEG$_4$-dimer over ^{99m}Tc-PEG$_4$-monomer; (2) assess the impact of an extra PEG$_4$ group on radiotracer excretion kinetics in kidneys, liver and lungs; and (3) compare the tumor uptake

of ^{99m}Tc-2PEG$_4$-dimer in the xenografted glioma and breast tumors. Figure 6 compares their tumor uptake and selected T/B ratios. Detailed biodistribution data for ^{99m}Tc-2PEG$_4$-dimer, ^{99m}Tc-3PEG$_4$-dimer and ^{99m}Tc-PEG$_4$-monomer are summarized in Tables SIII – SV.

The normal organ uptake of ^{99m}Tc-2PEG$_4$-dimer in the U87MG glioma-bearing mice was almost identical to that in mice bearing MDA-MB-435 breast cancer xenografts. Its tumor uptake was 11.17 ± 1.96 %ID/g and 8.31 ± 2.31 %ID/g at 30 and 120 min p.i., respectively. ^{99m}Tc-3PEG$_4$-dimer also had a high tumor uptake (8.17 ± 0.68 %ID/g and 9.74 ± 3.22 %ID/g at 30 and 120 min p.i., respectively) with very fast blood clearance (1.02 ± 0.22 %ID/g at 30 min p.i. and 0.17 ± 0.02 %ID/g at 120 min p.i.). Its kidney uptake was 17.60 ± 0.73 %ID/g at 30 min p.i. and 9.89 ± 1.20 % ID/g at 120 min p.i. Its liver uptake was 3.14 ± 0.18 %ID/g and 2.92 ± 0.77 %ID/g at 30 and 120 min p.i., respectively. At 30 min p.i., its muscle uptake (1.45 ± 0.20 %ID/g) was lower than that of ^{99m}Tc-2PEG$_4$-dimer (2.18 ± 0.37 %ID/g); but this difference diminished (1.00 ± 0.22 %ID/g for ^{99m}Tc-3PEG$_4$-dimer and 1.27 ± 0.20 %ID/g for ^{99m}Tc-2PEG$_4$-dimer) at 120 min p.i. The tumor/liver ratios of ^{99m}Tc-2PEG$_4$-dimer and ^{99m}Tc-3PEG$_4$-dimer were almost identical (Figure 6), but ^{99m}Tc-3PEG$_4$-dimer had better ($p < 0.01$) tumor/blood and tumor/muscle ratios than those of ^{99m}Tc-2PEG$_4$-dimer at 120 min p.i. The tumor uptake of ^{99m}Tc-PEG$_4$-monomer was 4.74 ± 2.71 %ID/g and 3.08 ± 0.83 %ID/g at 30 and 120 min p.i., respectively, and was much lower than that of ^{99m}Tc-2PEG$_4$-dimer and ^{99m}Tc-3PEG$_4$-dimer (Figure 6). As a result, its tumor/blood (3.85 ± 2.47 at 30 min p.i. and 15.50 ± 5.47 at 120 min p.i.) and tumor/liver (1.47 ± 0.91 at 30 min p.i. and 1.55 ± 0.38 at 120 min p.i.) ratios were lower ($p < 0.01$) than those of ^{99m}Tc-2PEG$_4$-dimer (tumor/blood = 9.63 ± 1.32 at 30 min p.i. and 29.12 ± 8.54 at 120 min p.i.; and tumor/liver = 2.59 ± 0.45 at 30 min p.i. and 3.33 ± 0.64 at 120 min p.i.) and ^{99m}Tc-3PEG$_4$-dimer (tumor/blood = 6.72 ± 2.88 at 30 min p.i. and 48.84 ± 18.74 at 120 min p.i.; and tumor/liver = 2.13 ± 0.87 at 30 min p.i. and 3.49 ± 1.64 at 120 min p.i.). The kidney uptake of ^{99m}Tc-PEG$_4$-monomer (10.78 ± 1.82 %ID/g at 30 min p.i. and 4.04 ± 0.69 % ID/g at 120 min p.i., respectively) was only half of that of ^{99m}Tc-2PEG$_4$-dimer (20.81 ± 2.32 %ID/g at 30 min p.i. and 10.21 ± 1.37 %ID/g at 120 min p.i.) and ^{99m}Tc-3PEG$_4$-dimer (17.60 ± 0.73 %ID/g at 30 min p.i. and 9.89 ± 1.20 %ID/g at 120 min p.i.). The muscle uptake of ^{99m}Tc-PEG$_4$-monomer (1.65 ± 0.25 %ID/g at 30 min p.i. and 0.62 ± 0.15 %ID/g at 120 min p.i.) was favorably compared to that of ^{99m}Tc-3PEG$_4$-dimer (1.45 ± 0.20 %ID/g at 30 min p.i. and 0.89 ± 0.10 %ID/g at 120 min p.i.) and within the experimental error.

Effect of Tumor Size

During biodistribution studies, we noticed that there is often a large variation in tumor size even if the same number of U87MG glioma cells were used for the same animal. In our previous report,[62] we found that smaller tumors (< 0.5 g) had higher radiotracer uptake than large tumors regardless of the identity of radiotracers. To further clarify the relationship between tumor uptake and tumor size, we added four extra glioma-bearing mice (tumor size = 0.4 – 1.7 g) into the 120 min group of ^{99m}Tc-3PEG$_4$-dimer. We found a linear relationship (Figure 5A) between the tumor size and %ID tumor uptake of ^{99m}Tc-3PEG$_4$-dimer with $R^2 = 0.9164$ for the eight tumor-bearing mice. As the tumor size increased, its %ID tumor uptake also increased in a linear fashion. If the tumor uptake is expressed as %/ID/g (Figure 5B), it appears that ^{99m}Tc-3PEG$_4$-dimer had a narrow window to achieve the optimal tumor uptake. When the tumor size was in the range of 0.1 g – 0.5 g (100 – 500 mm^3), its tumor uptake was 6.0 – 12.5 %ID/g. When the tumor size was too big (0.5 g – 1.6 g or 500 – 1700 mm^3), the tumor uptake was in the range of 4.0 – 6.0 %ID/g. When the tumor size was too small (<0.05 g or <50 mm^3), the tumor uptake of ^{99m}Tc-3PEG$_4$-dimer was only 2.0 – 4.0 %ID/g.

Metabolic Properties

Normal athymic nude mice were used to examine the metabolic stability of [99mTc]-PEG$_4$-monomer, [99mTc]-2PEG$_4$-dimer and [99mTc]-3PEG$_4$-dimer. Figure 8 shows typical radio-HPLC chromatograms of [99mTc]-2PEG$_4$-dimer in saline (A), in urine at 30 min p.i. (B) and 120 min p.i. (C), and in feces at 120 min p.i. (D). There was very little metabolite detected in either urine or feces over the 2 h period. [99mTc]-2PEG$_4$-dimer remained intact during its excretion from both renal and hepatobiliary routes. A similar metabolic stability was observed for the [99mTc]-PEG$_4$-monomer (Figure SI). However, the [99mTc]-3PEG$_4$-dimer had ~30% metabolism during its excretion from the hepatobiliary route, whereas it remained intact during its excretion from the renal route (Figure SII).

Planar Imaging

Figure 9 illustrates static images of the tumor-bearing mice administered with [99mTc]-3PEG$_4$-dimer at 30, 60, 120 and 240 min p.i. The glioma tumors were clearly visualized as early as 15 min p.i. with excellent contrast. No significant radioactivity accumulation was detected in the heart, liver and lungs. At >120 min p.i., the most visible organs are tumors, kidneys and bladder. The breast tumors with a similar size were also clearly visualized with high T/B contrast. The tumor uptake of [99mTc]-3PEG$_4$-dimer was significantly blocked (Figure 10A) by co-injection of excess E[c(RGDfK)]$_2$, suggesting that its tumor localization was indeed integrin $\alpha_v\beta_3$–specific. Figure 10B compares the 60 min static images of the athymic nude mice bearing U87MG glioma xenografts (tumor size ranging from 0.14 g to 0.85 g or 5 mm – 10 mm in diameter) administered with [99mTc]-3PEG$_4$-dimer. It was found that the tumors of ~5 mm in diameter could be readily visualized as soon as [99mTc]-3PEG$_4$-dimer was injected. Larger tumors (>350 mm^3 or >7 mm in diameter) had much better visualization than the smaller ones (<100 mm^3 or <5 mm in diameter) even though the %ID/g tumor uptake in larger tumors (400 – 1000 mm^3) was lower than those smaller ones (100 – 300 mm^3).

DISCUSSION

Many multimeric cyclic RGD peptides have been successfully used to develop the integrin $\alpha_v\beta_3$-targeted radiotracers.[31–36,49–62] For example, Liu et al have been using cyclic RGD dimers, such as E[c(RGDfK)]$_2$, to develop diagnostic and therapeutic radiotracers.[31,33–35] Chen and coworkers have been using E[c(RGDyK)]$_2$ and E{E[c(RGDyK)]$_2$}$_2$ to prepare the integrin $\alpha_v\beta_3$-targeted [64Cu] PET radiotracers.[51,56,71] Kessler et al reported the HEG (hexaethylene glycolic acid) and poly(lysine)-tethered cyclic RGDfE dimers and tetramers with integrin $\alpha_v\beta_3$ binding affinity better than their monomeric analogs.[49,50] HEG or poly(lysine) linkers were used to increase the distance between the adjacent cyclic RGDfE motifs. In this study, we determined the integrin $\alpha_v\beta_3$ binding affinities of HYNIC-2PEG$_4$-dimer and HYNIC-3PEG$_4$-dimer by competitive displacement of [125I]-c(RGDyK) bound to U87MG glioma cells (Figure 3). We found that the integrin $\alpha_v\beta_3$ binding affinity of HYNIC conjugates follows the order of HYNIC-2PEG$_4$-dimer ~ HYNIC-3PEG$_4$-dimer ~ HYNIC-tetramer > HYNIC-PEG$_4$-dimer > HYNIC-PEG$_4$-monomer ~ c(RGDyK). The addition of PEG$_4$ linkers between two cyclic RGD motifs in HYNIC-2PEG$_4$-dimer and HYNIC-3PEG$_4$-dimer significantly increased their integrin $\alpha_v\beta_3$ binding affinity. However, the addition of an extra PEG$_4$ linker between HYNIC and 2PEG$_4$-dimer had little impact on the integrin $\alpha_v\beta_3$ binding affinity. It is very important to note that the IC$_{50}$ value depends largely on the radioligand ([125I]-c(RGDyK) vs. [125I]-echistatin) and tumor cell lines (U87MG vs. MDA-MB-435) used in the competitive displacement assay. Caution should be taken when comparing the IC$_{50}$ values of cyclic RGD peptides with those reported in the literature.

The distance between the two RGD motifs in 2PEG$_4$-dimer is 38 bonds, whereas the longest distance between RGD motifs in E[c(RGDfK)]$_2$ is only 6 bonds (excluding side arms of K-

residues). The lower integrin $\alpha_v\beta_3$ binding affinity of HYNIC-PEG$_4$-dimer (IC$_{50}$ = 7.5 ± 2.3 nM) than that of HYNIC-2PEG$_4$-dimer (IC$_{50}$ = 2.9 ± 0.7 nM) strongly suggests that the distance between two cyclic RGD motifs in E[c(RGDfK)]$_2$ is too short for simultaneous integrin $\alpha_v\beta_3$ binding. Thus, the higher integrin $\alpha_v\beta_3$ binding affinity of HYNIC-PEG$_4$-dimer (IC$_{50}$ = 7.5 ± 2.3 nM) than that of HYNIC-PEG$_4$-monomer (IC$_{50}$ = 31.7 ± 9.7 nM) is caused by the "enhanced local RGD concentration" (Figure 1B). This might also explain the higher tumor uptake for the radiolabeled (^{18}F, ^{99m}Tc, ^{111}In and ^{64}Cu) cyclic RGD dimers (E[c(RGDfK)]$_2$ and E[c(RGDyK)]$_2$) as compared to their monomeric analogs.[51,52,54–62,72]

The longest distance between adjacent cyclic RGD motifs in the tetramer E[E[c(RGDfK)]$_2$]$_2$ is 16 bonds (excluding side arms of K-residues). HYNIC-tetramer has an integrin $\alpha_v\beta_3$ binding affinity (IC$_{50}$ = 2.8 ± 0.5 nM) almost identical to those of HYNIC-2PEG$_4$-dimer (IC$_{50}$ = 2.9 ± 0.7 nM) and HYNIC-3PEG$_4$-dimer (IC$_{50}$ = 2.4 ± 0.7 nM). However, it is not clear if its higher binding affinity than that of HYNIC-PEG$_4$-dimer (IC$_{50}$ = 7.5 ± 2.3 nM) is caused by the simultaneous integrin $\alpha_v\beta_3$ binding (Figure 1A) of two adjacent cyclic RGD motifs or is simply due to the presence of four cyclic RGD motifs in E[E[c(RGDfK)]$_2$]$_2$. It must be noted that the ability of a multimeric RGD peptide to achieve simultaneous integrin $\alpha_v\beta_3$ binding depends largely on integrin $\alpha_v\beta_3$ density. If the density is high, the distance between two neighboring integrin $\alpha_v\beta_3$ sites will be short enough so that it is much easier for the multimeric RGD peptide to achieve simultaneous integrin $\alpha_v\beta_3$ binding. If the integrin $\alpha_v\beta_3$ density is low, the distance between two neighboring integrin $\alpha_v\beta_3$ sites will be long, and it might be more difficult for the same multimeric RGD peptide to achieve simultaneous integrin $\alpha_v\beta_3$ binding.

The integrin $\alpha_v\beta_3$ binding affinity difference between HYNIC-2PEG$_4$-dimer and HYNIC-PEG$_4$-dimer is also reflected by the tumor uptake of their corresponding ternary ligand ^{99m}Tc complexes, [99m]Tc-2PEG$_4$-dimer and ^{99m}Tc-PEG$_4$-dimer. The fact that [99m]Tc-2PEG$_4$-dimer has twice the tumor uptake as ^{99m}Tc-PEG$_4$-dimer (Figure 4) in the same animal model with similar tumor size (100 – 500 m^3) provides direct in vivo evidence to support our conclusion that the two cyclic RGD motifs in 2PEG$_4$-dimer are indeed able to achieve simultaneous integrin $\alpha_v\beta_3$ binding while PEG$_4$-dimer is "monodentate" due to the short distance between its two cyclic RGD motifs. If they were bound to integrin $\alpha_v\beta_3$ in the same fashion, [99m]Tc-2PEG$_4$-dimer and ^{99m}Tc-PEG$_4$-dimer would have had similar tumor uptake in the same tumor-bearing animal model. Therefore, 2PEG$_4$-dimer is a better targeting biomolecule than PEG$_4$-dimer for future development of integrin $\alpha_v\beta_3$-targeted radiotracers. Since ^{99m}Tc-tetramer has the tumor uptake very close to that of [99m]Tc-2PEG$_4$-dimer (Figure 4) in the same tumor-bearing animal model, one *might* suggest that the higher tumor uptake of ^{99m}Tc-tetramer as compared to that of ^{99m}Tc-PEG$_4$-dimer is caused by the simultaneous integrin $\alpha_v\beta_3$ binding of two adjacent cyclic RGDfK motifs in E{E[c(RGDfK)]$_2$}$_2$. Alternatively, it is also reasonable to believe that the higher tumor uptake of ^{99m}Tc-tetramer than that of ^{99m}Tc-PEG$_4$-dimer is due to the presence of four cyclic RGD motifs in E[E[c(RGDfK)]$_2$]$_2$.

Both [99m]Tc-2PEG$_4$-dimer and [99m]Tc-3PEG$_4$-dimer have advantages over ^{99m}Tc-tetramer with respect to their accumulation in non-cancerous organs. For example, the uptake of [99m]Tc-2PEG$_4$-dimer and [99m]Tc-3PEG$_4$-dimer in kidneys and liver was much lower ($p < 0.01$) than that of ^{99m}Tc-tetramer (Figure 4). As a result, their tumor/liver and tumor/kidney ratios are significantly better than those for ^{99m}Tc-tetramer. The higher kidney uptake of ^{99m}Tc-tetramer is probably caused by the presence of more R-residues in E{E[c(RGDfK)]$_2$}$_2$. In addition, the cost for the synthesis of E{E[c(RGDfK)]$_2$}$_2$ is much higher than both 2PEG$_4$-dimer and 3PEG$_4$-dimer. On the basis of these facts, we strongly believe that 2PEG$_4$-dimer and 3PEG$_4$-dimer are better targeting biomolecules than E{E[c(RGDfK)]$_2$}$_2$ for the future development of integrin $\alpha_v\beta_3$-targeted radiotracers.

The tumor uptake of ^{99m}Tc-2PEG$_4$-dimer is partially blocked (Figure 5) by co-injection of excess E[c(RGDfK)]$_2$, indicating that the tumor uptake of ^{99m}Tc-2PEG$_4$-dimer is integrin $\alpha_v\beta_3$-mediated. The uptake blockage in the eyes, heart, intestine, lungs, liver and spleen suggests that the accumulation of ^{99m}Tc-2PEG$_4$-dimer in these organs is also integrin $\alpha_v\beta_3$-mediated. This conclusion is supported by the immunohistopathological studies, which showed a strong positive staining of endothelial cells of small glomeruli vessels in the kidneys and weak staining in branches of the hepatic portal vein.[71,72]

The glioma uptake of ^{99m}Tc-2PEG$_4$-dimer (11.17 ± 1.96 %ID/g) is higher ($p < 0.01$) than that in breast tumor (5.20 ± 1.74 %ID/g) at 30 min p.i., which is consistent with the fact that U87MG glioma cells have a higher integrin $\alpha_v\beta_3$ expression than MDA-MB-435 breast tumor cells.[69,70] However, this difference disappears at 120 min p.i. (8.31 ± 2.31 %ID/g in glioma and 9.77 ± 2.66 %ID/g in breast tumor). The glioma uptake of ^{99m}Tc-3PEG$_4$-dimer is comparable to that of ^{99m}Tc-2PEG$_4$-dimer. The extra PEG$_4$ linker in 3PEG$_4$-dimer does not significantly change the tumor uptake, which is consistent with the similar integrin $\alpha_v\beta_3$ binding affinity for HYNIC-2PEG$_4$-dimer (IC$_{50}$ = 2.9 ± 0.7 nM) and HYNIC-3PEG$_4$-dimer (IC$_{50}$ = 2.4 ± 0.7 nM). The glioma uptake of ^{99m}Tc-3PEG$_4$-dimer is almost 3× better than that for ^{99m}Tc-PEG$_4$-monomer over the 2 h study period (Figure 6), further demonstrating the superiority of 3PEG$_4$-dimer over PEG$_4$-monomer as the integrin $\alpha_v\beta_3$-targeting biomolecules.

Non-invasive imaging of molecular markers, such as integrin $\alpha_v\beta_3$, is highly desirable for patient selection before anti-angiogenic treatment as it can provide more effective monitoring of therapeutic efficacy in the integrin $\alpha_v\beta_3$-positive cancer patients.[73] The %ID tumor uptake reflects the integrin $\alpha_v\beta_3$ expression level on tumor cells and tumor neovasculature while the %ID/g tumor uptake reflects the integrin $\alpha_v\beta_3$ density. When tumors are <0.05 g (~50 mm^3), there is little integrin $\alpha_v\beta_3$ expression. As a result, the tumor uptake (%ID and %ID/g) is low. When tumors are in the rapid growing stage (0.1 – 0.5 g or 100 – 500 mm^3), the microvessel and integrin $\alpha_v\beta_3$ density is higher. The radiotracer %ID/g tumor uptake is higher (Figure 5B) even though its %ID tumor uptake is low (Figure 5A). As tumors grow, the total number of integrin $\alpha_v\beta_3$ sites on tumor cells and tumor neovasculature becomes larger. As a result, the %ID tumor uptake increases (Figure 5A). However, the microvessel density decreases due to the maturation of blood vessels, and the integrin $\alpha_v\beta_3$ density also decreases due to larger interstitial space and higher collagen concentrations.[74] In addition, parts of the tumor may become necrotic, leading to the lower integrin $\alpha_v\beta_3$ density and the low radiotracer %ID/g uptake in larger tumors (Figure 5B).

Since tumors must have sufficient radioactivity counts to be detectable by planar or SPECT imaging, the total %ID tumor uptake is critically important for early tumor detection and noninvasive monitoring of the tumor growth or shrinkage during anti-angiogenic treatment in cancer patients. In this study, we found that tumors of ~5 mm in diameter are readily visualized with excellent contrast as early as 30 min p.i. At 60 min p.i., the only organs visible are tumors, kidneys and bladder of the tumor-bearing mouse (Figure 10B). Larger tumors have much better visualization than the smaller ones even though the %ID/g tumor uptake in larger tumors might be lower than that in smaller ones (Figure 8). The tumor detection limit is about 5 mm in diameter with ^{99m}Tc-3PEG$_4$-dimer as the radiotracer. These data clearly show that ^{99m}Tc-3PEG$_4$-dimer is very useful for early detection of the integrin $\alpha_v\beta_3$–positive tumors and has potential applications for noninvasive monitoring of the tumor growth or shrinkage during anti-angiogenic treatment.

Extensive metabolic degradation was observed for the ^{99m}Tc-labeled cyclic RGD monomer,[75] dimer,[58,60] tetramer,[53,54] and the ^{64}Cu-labeled cyclic RGD tetramer in the kidneys and urine samples.[56] In this study, we found that ^{99m}Tc-2PEG$_4$-dimer has very high metabolic stability during its excretion from both renal and hepatobiliary routes (Figure 6). Similar

metabolic stability is also observed for ^{99m}Tc-PEG$_4$-monomer (Figure SI). In contrast, ^{99m}Tc-3PEG$_4$-dimer has ~30% metabolism during its excretion from the hepatobiliary route (Figure SII). The metabolic stability difference between ^{99m}Tc-2PEG$_4$-dimer and ^{99m}Tc-3PEG$_4$-dimer is due to the extra PEG$_4$ in 3PEG$_4$-dimer. It remains unclear how the extra PEG$_4$ linker influences metabolic stability of the ^{99m}Tc-labeled cyclic RGD peptide dimers.

CONCLUSION

In this study, we evaluated two new radiotracers, ^{99m}Tc-2PEG$_4$-dimer and ^{99m}Tc-3PEG$_4$-dimer, for non-invasive imaging of tumor integrin $\alpha_v\beta_3$ expression in athymic nude mice bearing U87MG glioma and MDA-MB-435 breast cancer xenografts. We found that (1) the tumor-targeting capability could be significantly enhanced by addition of two PEG$_4$ linkers between two cyclic RGD motifs, which allow them to achieve simultaneous integrin $\alpha_v\beta_3$ binding; (2) PEG$_4$ linkers are particularly useful for improving the clearance kinetics of ^{99m}Tc-2PEG$_4$-dimer and ^{99m}Tc-3PEG$_4$-dimer from non-cancerous organs, such as the kidneys, liver and lungs; and (3) the %ID tumor uptake is correlated well with the tumor size in a linear fashion. ^{99m}Tc-3PEG$_4$-dimer has the best profile with respect to tumor uptake, T/B ratios and pharmacokinetics among the ^{99m}Tc-labeled cyclic RGD peptide dimers and tetramers evaluated in the xenografted U87MG glioma and MDA-MB-435 breast cancer animal models. In addition, ^{99m}Tc-3PEG$_4$-dimer can be readily prepared in high yield and radiochemical purity (RCP >95%) with very high specific activity (>5 mCi/μg or 10 Ci/μmol) from a single-vial kit formulation. ^{99m}Tc-3PEG$_4$-dimer has significant advantages over the ^{18}F-labeled cyclic RGD peptides with respect to cost, availability and easiness of routine clinical preparation. All these factors make ^{99m}Tc-3PEG$_4$-dimer a very attractive SPECT radiotracer for the early detection of integrin $\alpha_v\beta_3$–positive tumors and for noninvasive monitoring of tumor growth or treatment efficacy in clinical settings.

Supplementary Material

Refer to Web version on PubMed Central for supplementary material.

Acknowledgements

References

1. Folkman J. Angiogenesis in cancer, vascular, rheumatoid and other disease. Nat Med 1995;1:27–31. [PubMed: 7584949]

2. Mousa SA. Mechanism of angiogenesis in vascular disorders: potential therapeutic targets. Drugs of the Future 1998;23:51–60.

3. Carmeliet P. Mechanisms of angiogenesis and arteriogenesis. Nat Med 2000;6:389–395. [PubMed: 10742145]

4. Meitar D, Crawford SE, Rademaker AW, Cohn SL. Tumor angiogenesis correlates with metastatic disease, N-*myc*-amplification, and poor outcome in human neuroblastoma. J Clinical Oncol 1996;14:405–414. [PubMed: 8636750]

5. Gasparini G, Brooks PC, Biganzoli E, Vermeulen PB, Bonoldi E, Dirix LY, Ranieri G, Miceli R, Cheresh DA. Vascular integrin $\alpha_v\beta_3$: a new prognostic indicator in breast cancer. Clinical Can Res 1998;4:2625–2634.

6. Falcioni R, Cimino L, Gentileschi MP, D'Agnano I, Zupi G, Kennel SJ, Sacchi A. Expression of beta 1, beta 3, beta 4, and beta 5 integrins by human lung carcinoma cells of different histotypes. Exp Cell Res 1994;210:113–122. [PubMed: 7505746]

7. Sengupta S, Chattopadhyay N, Mitra A, Ray S, Dasgupta S, Chatterjee A. Role of $\alpha_v\beta_3$ integrin receptors in breast tumor. J Exp Clin Cancer Res 2001;20:585–590. [PubMed: 11876555]

8. Zitzmann S, Ehemann V, Schwab M. Arginine-Glycine-Aspartic acid (RGD)-peptide binds to both tumor and tumor endothelial cells in vivo. Cancer Res 2002;62:5139–5143. [PubMed: 12234975]

9. Weber WA, Haubner R, Vabuliene E, Kuhnast B, Webster HJ, Schwaiger M. Tumor angiogenesis targeting using imaging agents. Q J Nucl Med 2001;45:179–182. [PubMed: 11476168]

10. Costouros NG, Diehn FE, Libutti SK. Molecular imaging of tumor angiogenesis. J Cell Biol Suppl 2002;39:72–78.

11. Liu S, Edwards DS. Fundamentals of receptor-based diagnostic metalloradiopharmaceuticals. Topics in Current Chem 2002;222:259–278.

12. Van de Wiele C, Oltenfreiter R, De Winter O, Signore A, Slegers G, Dieckx RA. Tumor angiogenesis pathways: related clinical issues and implications for nuclear medicine imaging. Eur J Nucl Med Mol Imag 2002;29:699–709.

13. van, Hinsbergh VWM.; Collen, A.; Koolwijk, P. Angiogenesis and antiangiogenesis: perspectives for the treatment of solid tumors. Ann Oncol 1999;4:S60–S63.

14. Brower V. Tumor angiogenesis-new drug on the block. Nature Biol 1999;17:963–968.

15. Brooks PC, Montgomery AMP, Rosenfeld M, Reisenfeld R, Hu T, Klier G, Cheresh DA. Integrin $\alpha_v\beta_3$ antagonists promote tumor regression by inducing apoptosis of angiogenic blood vessels. Cell 1994;79:1157–1164. [PubMed: 7528107]

16. Giannis A, Rübsam F. Integrin antagonists and other low molecular weight compounds as inhibitors of angiogenesis: new drugs in cancer therapy. Angew Chem Int Ed Engl 1997;36:588–590.

17. Haubner R, Finsinger D, Kessler H. Stereoisomeric peptide libraries and peptidomimetics for designing selective inhibitors of the $\alpha_v\beta_3$ integrin for a new cancer therapy. Angew Chem Int Ed Engl 1997;36:1374–1389.

18. Gottschalk KE, Kessler H. The structure of integrins and integrin-ligand complexes: Implications for drug design and signal transduction. Angew Chem Int Ed Engl 2002;41:1374–1389.

19. Burke PA, DeNardo SJ. Antiangiogenic agents and their promising potential for combined therapy. Cancer Res 2001;48:7022–7032.

20. Qiao R, Yan W, Lum H, Malik AB. Arg-Gly-Asp peptide increases endothelial hydraulic conductivity: comparison with thrombin response. Am J Physiol 1995;268:C110–C117. [PubMed: 7631737]

21. Huabner R, Wester HJ, Senekowitsch-Schmidtke R, Diefenbach B, Kessler H, Stöcklin G, Schwaiger M. RGD-peptides for tumor targeting: biological evaluation of radioiodinated analogs and introduction of a novel glycosylated peptide with improved biokinetics. J Labelled Compounds & Radiopharmaceuticals 1997;40:383–385.

22. Sivolapenko GB, Skarlos D, Pectasides D, Stathopoulou E, Milonakis A, Sirmalis G, Stuttle A, Courtenay-Luck NS, Konstantinides K, Epenetos AA. Imaging of metastatic melanoma utilizing a technetium-99m labeled RGD-containing synthetic peptide. Eur J Nucl Med 1998;25:1383–1389. [PubMed: 9818277]

23. Haubner R, Wester HJ, Reuning U, Senekowisch-Schmidtke R, Diefenbach B, Kessler H, Stöcklin G, Schaiger M. Radiolabeled $\alpha_v\beta_3$ integrin antagonists: a new class of tracers for tumor targeting. J Nucl Med 1999;40:1061–1071. [PubMed: 10452325]

24. Haubner R, Wester HJ, Weber WA, Mang C, Ziegler SI, Goodman SL, Senekowisch-Schmidtke R, Kessler H, Schwaiger M. Noninvasive imaging of $\alpha_v\beta_3$ integrin expression using ^{18}F-labeled RGD-containing glycopeptide and positron emission tomography. Cancer Res 2001;61:1781–1785. [PubMed: 11280722]

25. Haubner R, Wester HJ, Burkhart F, Senekowisch-Schmidtke R, Weber W, Goodman SL, Kessler H, Schwaiger M. Glycosylated RGD-containing peptides: tracer for tumor targeting and angiogenesis imaging with improved biokinetics. J Nucl Med 2001;42:326–336. [PubMed: 11216533]

26. Poethko T, Schottelius M, Thumshirn G, Hersel U, Herz M, Henriksen G, Kessler H, Schaiger M, Wester HJ. Two-step methodology for high yield routine radiohalogenation of peptides: ^{18}F-labeled RGD and octreotide analogs. J Nucl Med 2004;45:892–902. [PubMed: 15136641]

27. Chen X, Park R, Tohme M, Shahinian AH, Bading JR, Conti PS. MicroPET and autoradiographic imaging of breast cancer α_v-integrin expression using [18]F- and ^{64}Cu-labeled RGD peptide. Bioconj Chem 2004;15:41–49.

28. Chen X, Shahinian A, Park R, Bozorgzadeh MH, Bading JR, Conti PS. ^{18}F-labeled cyclic RGD peptide for PET imaging of tumor angiogenesis. J Nucl Med 2003;44(5 Suppl):47–48.

29. Chen X, Park R, Shahinian AH, Tohme M, Khankaldyyan V, Bozorgzadeh MH, Bading JR, Moats R, Laug WE, Conti PS. ^{18}F-labeled RGD peptide: initial evaluation for imaging brain tumor angiogenesis. Nucl Med Biol 2004;31:179–189. [PubMed: 15013483]

30. Chen X, Park R, Shahinian AH, Bading JR, Conti PS. Pharmacokinetics and tumor retention of ^{125}I-labeled RGD peptide are improved by PEGylation. Nucl Med Biol 2004;31:11–19. [PubMed: 14741566]

31. Liu S, Edwards DS, Ziegler MC, Harris AR, Hemingway SJ, Barrett JA. ^{99m}Tc-Labeling of a hydrazinonicotinamide-conjugated vitronectin receptor antagonist useful for imaging tumors. Bioconj Chem 2001;12:624–629.

32. Dijkgraaf I, Rijinders AY, Soede A, Dechesne AC, van Esse GW, Brouwer AJ, Corstens FHM, Boerman OC, Rijkers DTS, Liskamp RMJ. Synthesis of DOTA-conjugated multivalent cyclic-RGD peptide dendrimers via 1,3-dipolar cycloaddition and their biological evaluation: implications for tumor-targeting and tumor imaging purposes. Org Biomol Chem 2007;5:935–944. [PubMed: 17340009]

33. Liu S, Cheung E, Rajopadhye M, Ziegler MC, Edwards DS. [90]Y- and ^{177}Lu-labeling of a DOTA-conjugated vitronectin receptor antagonist for tumor therapy. Bioconj Chem 2001;12:559–568.

34. Janssen M, Oyen WJG, Massuger LFAG, Frielink C, Dijkgraaf I, Edwards DS, Rajopadyhe M, Corsten FHM, Boerman OC. Comparison of a monomeric and dimeric radiolabeled RGD-peptide for tumor targeting. Cancer Biother & Radiopharm 2002;17:641–646.

35. Janssen M, Oyen WJG, Dijkgraaf I, Massuger LFAG, Frielink C, Edwards DS, Rajopadyhe M, Boonstra H, Corsten FH, Boerman OC. Tumor targeting with radiolabeled integrin $\alpha_v\beta_3$ binding peptides in a nude mouse model. Cancer Res 2002;62:6146–6151. [PubMed: 12414640]

36. Line BR, Mitra A, Nan A, Ghandehari H. Targeting tumor angiogenesis: comparison of peptide and polymer-peptide conjugates. J Nucl Med 2005;46:1552–1560. [PubMed: 16157540]

37. Liu S, Robinson SP, Edwards DS. Integrin $\alpha_v\beta_3$ directed radiopharmaceuticals for tumor imaging. Drugs of the Future 2003;28:551–564.

38. Haubner R, Wester HJ. Radiolabeled tracers for imaging of tumor angiogenesis and evaluation of antiangiogenic therapies. Curr Pharm Design 2004;10:1439–1455.

39. D'Andrea LD, Del Gatto A, Pedone C, Benedetti E. Peptide-based molecules in angiogenesis. Chem Biol Drug Desgin 2006;67:115–126.

40. Meyer A, Auremheimer J, Modlinger A, Kessler H. Targeting RGD recognizing integrins: drug development biomaterial research tumor, imaging and targeting. Curr Pharm Design 2006;12:2723–2747.

41. Chen X. Multimodality imaging of tumor integrin $\alpha_v\beta_3$ expression. Mini-Rev Med Chem 2006;6:227–234. [PubMed: 16472190]

42. Cai W, Chen X. Multimodality imaging of tumor angiogenesis. J Nucl Med 2008;49:113S–128S. [PubMed: 18523069]

43. Liu S. Radiolabeled multimeric cyclic RGD peptides as integrin $\alpha_v\beta_3$-targeted radiotracers for tumor imaging. Mol Pharm 2006;3:472–487. [PubMed: 17009846]

44. Kenny LM, Coombes RC, Oulie I, Contractor KB, Miller M, Spinks TJ, McParland B, Cohen PS, Hui A, Palmieri C, Osman S, Glaser M, Turton D, Al-Nahhas A, Anoagye EO. Phase I trial of the positron-emitting Arg-Gly-Asp (RGD) peptide radioligand ^{18}F-AH111585 in breast cancer patients. J Nucl Med 2008;49:879–886. [PubMed: 18483090]

45. Beer AJ, Haubner R, Goebel M, Luderschmidt S, Spilker ME, Wester HJ, Weber WA, Schwaiger M. Biodistribution and pharmacokineticss of the $\alpha_v\beta_3$-selective tracer ^{18}F-Galacto-RGD in cancer patients. J Nucl Med 2005;46:1333–1341. [PubMed: 16085591]

46. Haubner R, Weber WA, Beer AJ, Vabulience E, Reim D, Sarbia M, Becker KF, Goebel M, Hein R, Wester HJ, Kessler H, Schwaiger M. Noninvasive visualization of the activated $\alpha_v\beta_3$ integrin in cancer patients by positron emission tomography and [^{18}F]Galacto-RGD. PLOS Medicine 2005;2:e70, 244–252. [PubMed: 15783258]

47. Boturyn D, Coll JL, Garanger E, Favrot MC, Dumy P. Template assembled cyclopeptides as multimeric system for integrin targeting and endocytosis. J Am Chem Soc 2004;126:5730–5739. [PubMed: 15125666]

48. Mammen M, Choi SK, Whitesides GM. Polyvalent interactions in biological systems: implications for design and use of multivalent ligands and inhibitors. Angew Chem Int Ed 1998;37:2755–2794.

49. Poethko T, Thumshirn G, Hersel U, Rau F, Haubner R, Schwaiger M. Improved tumor uptake, tumor retention and tumor/background ratios of pegylated RGD multimers. J Nucl Med 2003;44:46P.

50. Thumshirn G, Hersel U, Goodman SL, Kessler H. Multimeric cyclic RGD peptides as potential tools for tumor targeting: solid-phase peptide synthesis and chemoselective oxime ligation. Chem Eur J 2003;9:2717–2725.

51. Chen X, Liu S, Hou Y, Tohme M, Park R, Bading JR, Conti PS. MicroPET imaging of breast cancer integrin $\alpha_v\beta_3$ expression with ^{64}Cu-labeled dimeric RGD-containing cyclic peptides. Mol Imag Biol 2004:350–359.

52. Chen X, Tohme M, Park R, Hou Y, Bading JR, Conti PS. MicroPET imaging of breast cancer α_v-integrin expression with ^{18}F-labeled dimeric RGD peptide. Mol Imaging 2005;3:96–104. [PubMed: 15296674]

53. Liu S, Hsieh WY, Jiang Y, Kim YS, Sreerama SG, Chen X, Jia B, Wang F. Evaluation of a ^{99m}Tc-labeled cyclic RGD tetramer for noninvasive imaging integrin $\alpha_v\beta_3$-positive breast cancer. Bioconj Chem 2007;18:438–446.

54. Liu S, Kim YS, Hsieh WY, Sreerama SG. Coligand effects on solution stability, biodistribution and metabolism of ^{99m}Tc-labeled cyclic RGDfK tetramer. Nucl Med Biol 2008;35:111–121. [PubMed: 18158950]

55. Jia B, Liu Z, Liu ZF, Yu ZL, Zhi Yang Z, Zhao HY, He ZJ, Liu S, Wang F. Linker effects on biological properties of ^{111}In-labeled DTPA conjugates of a cyclic RGDfK dimer. Bioconj Chem 2008;19:201–210.

56. Wu Y, Zhang X, Xiong Z, Cheng Z, Fisher DR, Liu S, Gambhir SS, Chen X. MicroPET imaging of glioma integrin $\alpha_v\beta_3$ expression using ^{64}Cu-labeled tetrameric RGD peptide. J Nucl Med 2005;46:1707–1718. [PubMed: 16204722]

57. Dijkgraaf I, Kruijtzer JAW, Liu S, Soede A, Oyen WJG, Corstens FHM, Liskamp RMJ, Boerman OC. Improved targeting of the $\alpha_v\beta_3$ integrin by multimerization of RGD peptides. Eur J Nucl Med Mol Imaging 2007;34:267–273. [PubMed: 16909226]

58. Liu S, Hsieh WY, Kim YS, Mohammed SI. Effect of coligands on biodistribution characteristics of ternary ligand ^{99m}Tc complexes of a HYNIC-conjugated cyclic RGDfK dimer. Bioconj Chem 2005;16:1580–1588.

59. Jia B, Shi J, Yang Z, Xu B, Liu Z, Zhao H, Liu S, Wang F. ^{99m}Tc-labeled cyclic RGDfK dimer: initial evaluation for SPECT imaging of glioma integrin $\alpha_v\beta_3$ expression. Bioconj Chem 2006;17:1069–1076.

60. Liu S, He ZJ, Hsieh WY, Kim YS, Jiang Y. Impact of PKM linkers on biodistribution characteristics of the ^{99m}Tc-labeled cyclic RGDfK dimer. Bioconj Chem 2006;17:1499–1507.

61. Dijkgraaf I, Liu S, Kruijtzer JAW, Soede AC, Oyen WJG, Liskamp RMJ, Corstens FHM, Boerman OC. Effect of linker variation on the in vitro and in vivo characteristics of an ^{111}In-labeled RGD Peptide. Nucl Med Biol 2007;34:29–35. [PubMed: 17210459]

62. Wang JJ, Kim YS, Liu S. ^{99m}Tc-labeling of HYNIC-conjugated cyclic RGDfK dimer and tetramer using EDDA as coligand. Bioconj Chem 2008;19:634–642.

63. Liu S, Edwards DS, Barrett JA. ^{99m}Tc-labeling of highly potent small peptides. Bioconj Chem 1997;8:621–636.

64. Liu S, Edwards DS. ^{99m}Tc-labeled small peptides as diagnostic radiopharmaceuticals. Chem Rev 1999;99:2235–2268. [PubMed: 11749481]

65. Liu S. 6-Hydrazinonicotinamide derivatives as bifunctional coupling agents for ^{99m}Tc-labeling of small biomolecules. Topics in Current Chem 2005;252:117–153.

66. Harris TD, Sworin M, Williams N, Rajopadhye M, Damphousse PR, Glowacka D, Poirier MJ, Yu K. Synthesis of stable hydrazones of a hydrazinonicotinyl-modified peptide for the preparation of ^{99m}Tc-labeled radiopharmaceuticals. Bioconj Chem 1999;10:808–814.

67. Liu S, Edwards DS, Harris AR, Ziegler MC, Poirier MJ, Ewels BA, DiLuzio WR, Hui P. Towards developing a non-SnCl$_2$ formulation for RP444: a new radiopharmaceutical for thrombus imaging. J Pharm Sci 2001;90:114–123. [PubMed: 11169528]

68. Edwards DS, Liu S, Barrett JA, Harris AR, Looby RJ, Ziegler MC, Heminway SJ, Carroll TR. A new and versatile ternary ligand system for technetium radiopharmaceuticals: water soluble phosphines and tricine as coligands in labeling a hydrazino nicotinamide-modified cyclic glycoprotein IIb/IIIa receptor antagonist with ^{99m}Tc. Bioconj Chem 1997;8:146–154.

69. Liu S, Edwards DS, Harris AR. A novel ternary ligand system for ^{99m}Tc-labeling of hydrazinonicotinamide-modified biologically active molecules using imine-N containing heterocycles as coligands. Bioconj Chem 1998;9:583–595.

70. Liu S, Edwards DS, Harris AR, Heminway SJ, Barrett JA. Technetium complexes of a hydrazinonicotinamide-conjugated cyclic peptide and 2-hydrazinopyridine: Synthesis and characterization. Inorg Chem 1999;38:1326–1335. [PubMed: 11670921]

71. Wu Z, Li Z, Chen K, Cai W, He L, Chin FT, Li F, Chen X. Micro-PET of tumor integrin $\alpha_v\beta_3$ expression using ^{18}F-labeled PEGylated tetrameric RGD peptide (^{18}F-FPRGD4). J Nucl Med 2007;48:1536–1544. [PubMed: 17704249]

72. Zhang X, Xiong Z, Wu Y, Cai W, Tseng JR, Gambhir SS, Chen X. Quantitative PET imaging of tumor integrin $\alpha_v\beta_3$ expression with ^{18}F-FPRGD2. J Nucl Med 2006;47:113–121. [PubMed: 16391195]

73. Cai W, Rao J, Gambhir SS, Chen X. How molecular imaging is speeding up antiangiogenic drug development. Mol Cancer Ther 2006;5:2624–2633. [PubMed: 17121909]

74. Jain RK. Transport of molecules in the tumor interstitium: a review. Cancer Res 1987;47:3039–3051. [PubMed: 3555767]

75. Haubner R, Bruchertseifer F, Bock M, Schwaiger M, Wester HJ. Synthesis and biological evaluation of ^{99m}Tc-labeled cyclic RGD peptide for imaging integrin $\alpha_v\beta_3$ expression. Nuklearmedizin 2004;43:26–32. [PubMed: 14978538]
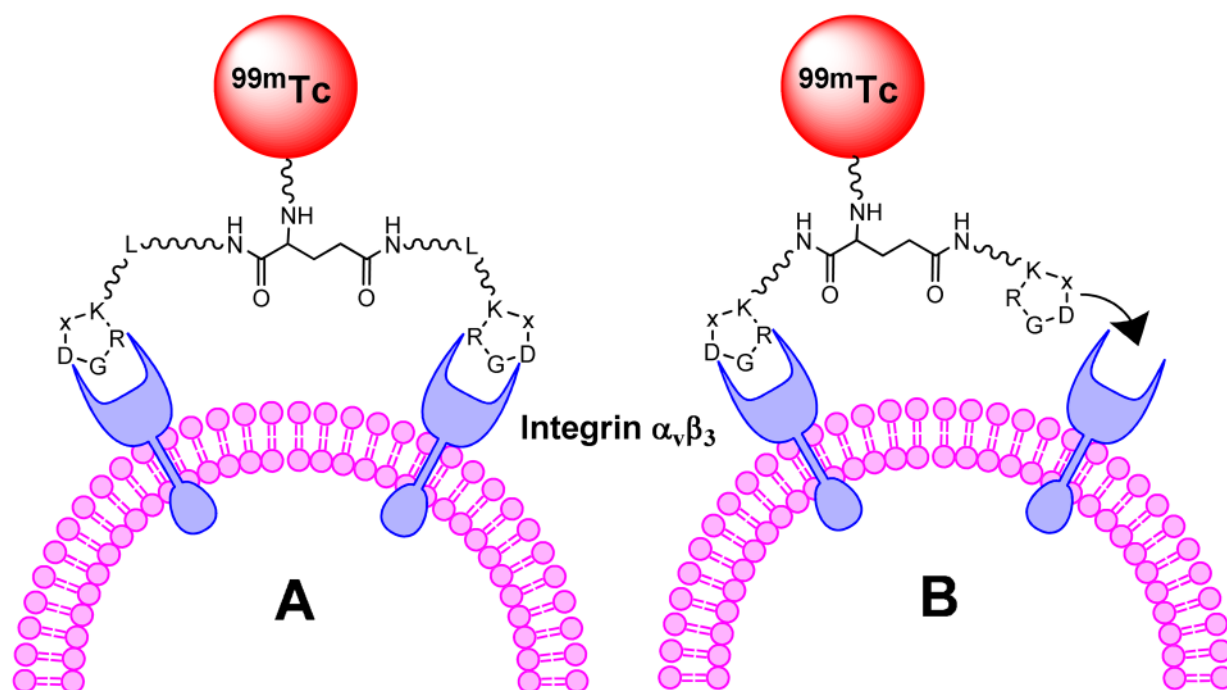
Figure 1.
Schematic illustration of interactions between the cyclic RGD peptide dimers and integrin $\alpha_v\beta_3$. **A**: the distance between two RGD motifs is long enough, and the multimeric cyclic peptide is able to bind integrin $\alpha_v\beta_3$ in a "bidentate" fashion. **B**: the distance between two cyclic RGD motifs is not long enough for simultaneous integrin $\alpha_v\beta_3$ binding, but the RGD concentration is "locally enriched" in the vicinity of neighboring integrin $\alpha_v\beta_3$ once the first cyclic RGD motif is bounded. In both cases, the result would be higher integrin $\alpha_v\beta_3$ binding affinity and slower dissociation kinetic from integrin $\alpha_v\beta_3$ of multimeric cyclic RGD peptides.

Figure 2.
HYNIC-conjugated cyclic RGD peptide dimers, HYNIC-PEG$_4$-c(RGDfK) (PEG$_4$-monomer),
HYNIC-PEG$_4$-E[c(RGDfK)]$_2$ (PEG$_4$-dimer), HYNIC-E[PEG$_4$-c(RGDfK)]$_2$ (2PEG$_4$-dimer),
HYNIC-PEG$_4$-E[PEG$_4$-c(RGDfK)]$_2$ (3PEG$_4$-dimer), and their ternary ligand ^{99m}Tc
complexes [^{99m}Tc(HYNIC-RGD)(tricine)(TPPTS)] (RGD = PEG$_4$-monomer, PEG$_4$-dimer,
2PEG$_4$-dimer and 3PEG$_4$-dimer).
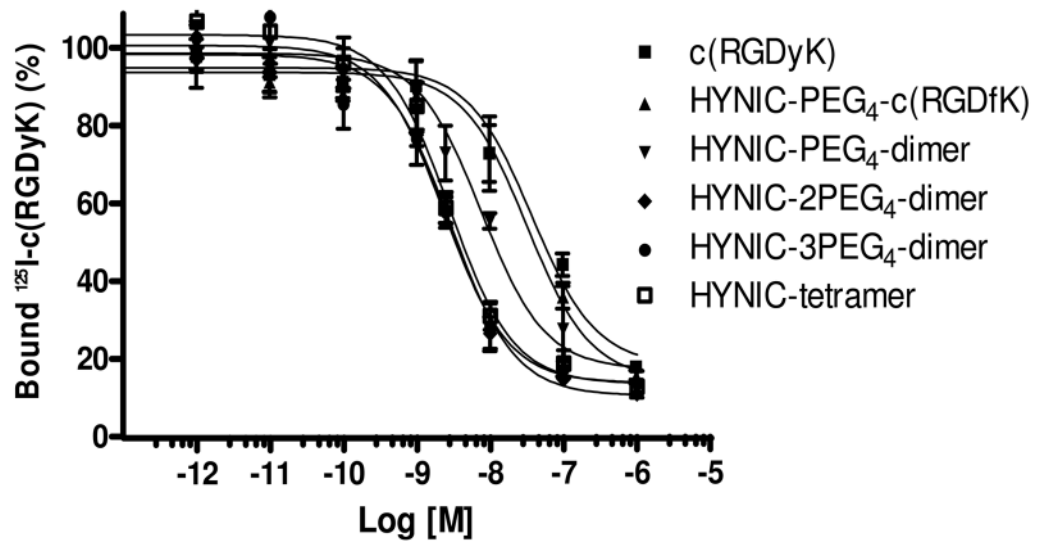
Figure 3.
In vitro inhibition curves of ^{125}I-c(RGDyK) bound to U87MG glioma cells by c(RGDyK), HYNIC-PEG$_4$-monomer, HYNIC-PEG$_4$-dimer, HYNIC-2PEG$_4$-dimer, HYNIC-3PEG$_4$-dimer and HYNIC-tetramer. Their IC$_{50}$ values were calculated to be 37 ± 5 nM, 32 ± 2 nM, 7.5 ± 0.5 nM, 2.9 ± 0.3 nM, 2.4 ± 0.3 nM and 2.8 ± 0.4 nM, respectively.
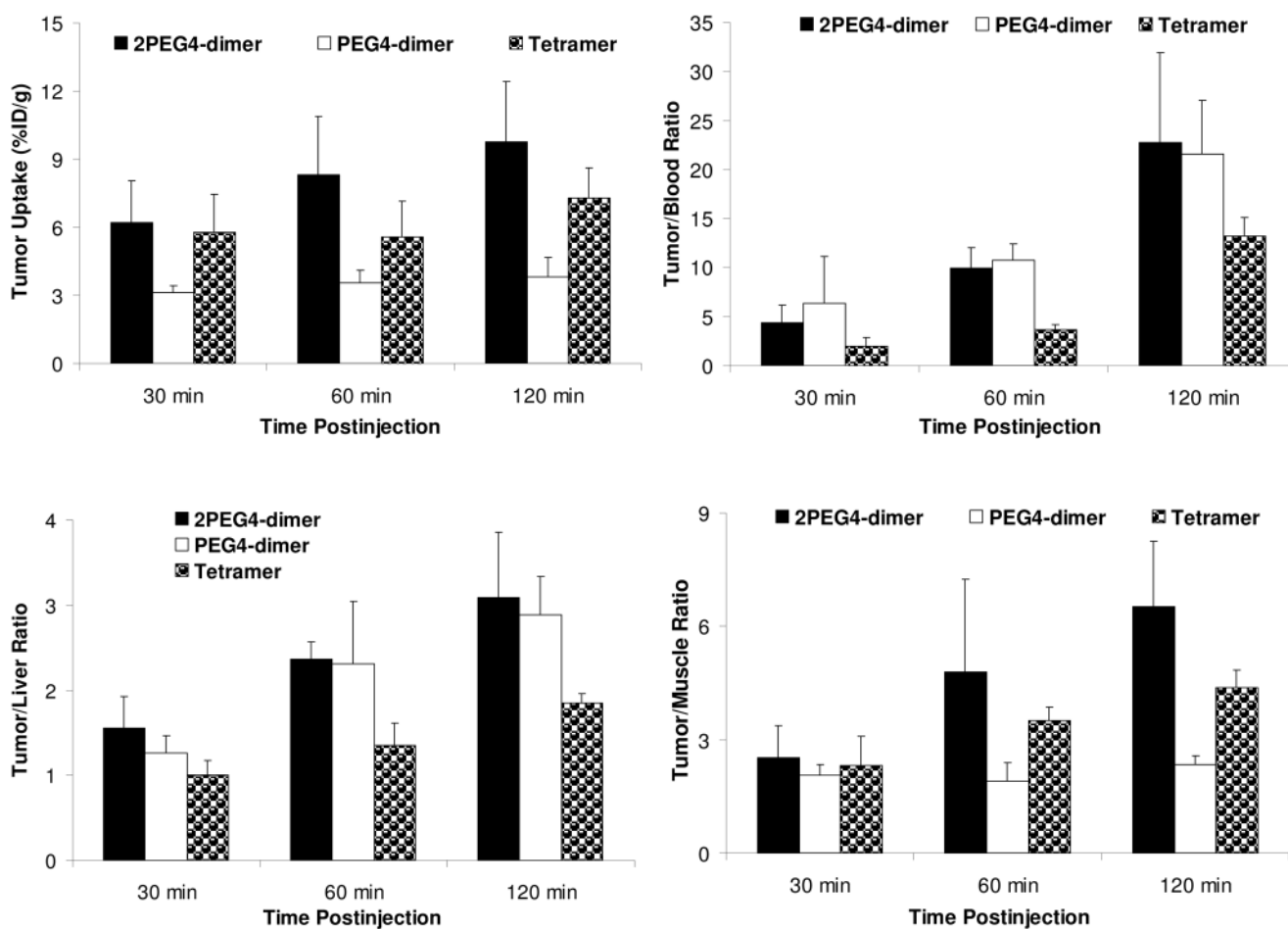
Figure 4.
Direct comparison of tumor uptake (%Id/g) and T/B ratios between ^{99m}Tc-2PEG$_4$-dimer, ^{99m}Tc-PEG$_4$-dimer and ^{99m}Tc-tetramer in athymic nude mice (n = 4) bearing MDA-MB-435 breast cancer xenografts.
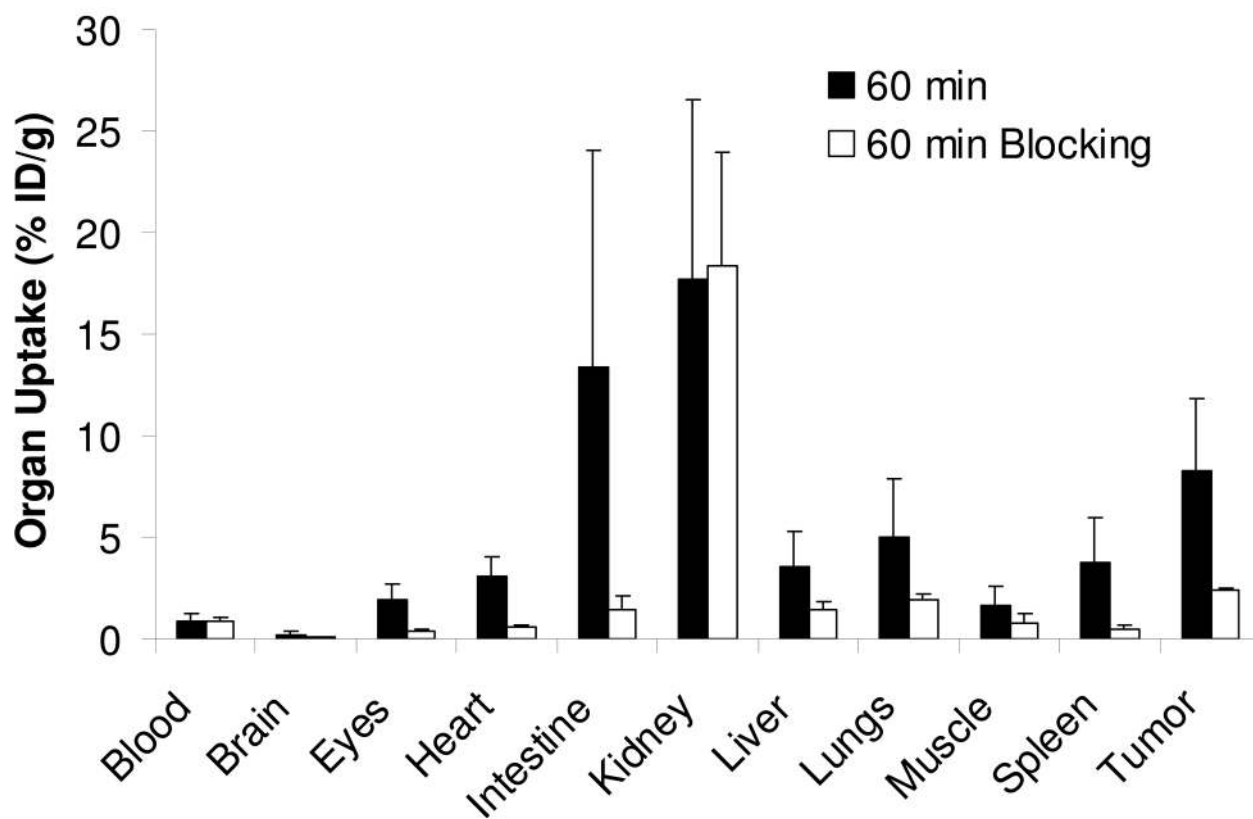
Figure 5.
Comparison of organ uptake for ^{99m}Tc-2PEG$_4$-dimer in the absence or presence of excess E
[c(RGDfK)]$_2$ at 60 min p.i.
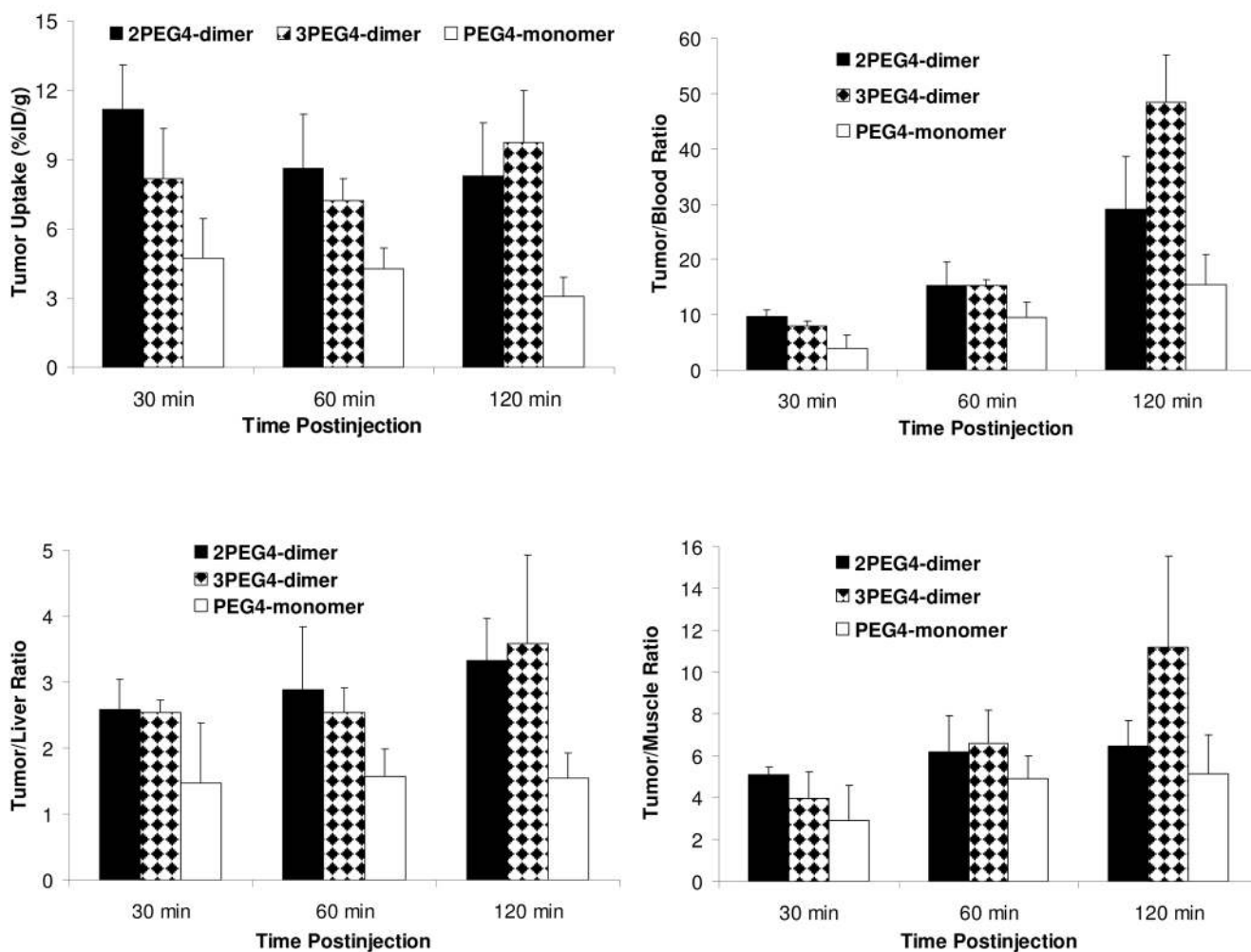
Figure 6.
Comparison of the tumor uptake (%ID/g) and T/B ratios between ^{99m}Tc-PEG_4-monomer, ^{99m}Tc-2PEG_4-dimer and ^{99m}Tc-3PEG_4-dimer in athymic nude mice (n = 4) bearing the U87MG glioma xenografts.
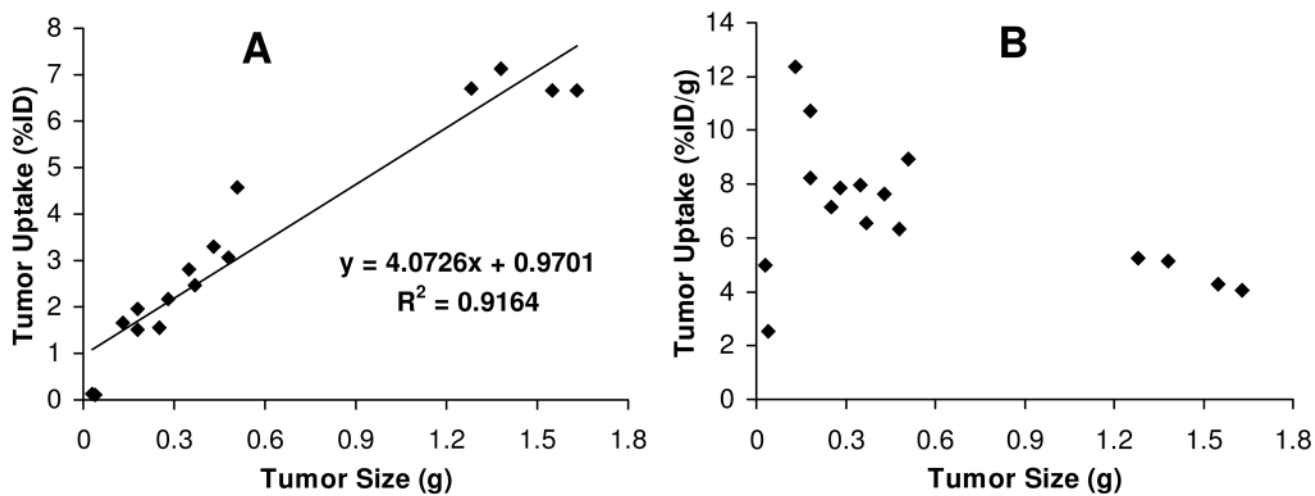
Figure 7.
The relationship between tumor size and tumor uptake of ^{99m}Tc-3PEG$_4$-dimer at 120 min p.i. in the athymic nude mice (n = 16) bearing the U87MG glioma xenografts.
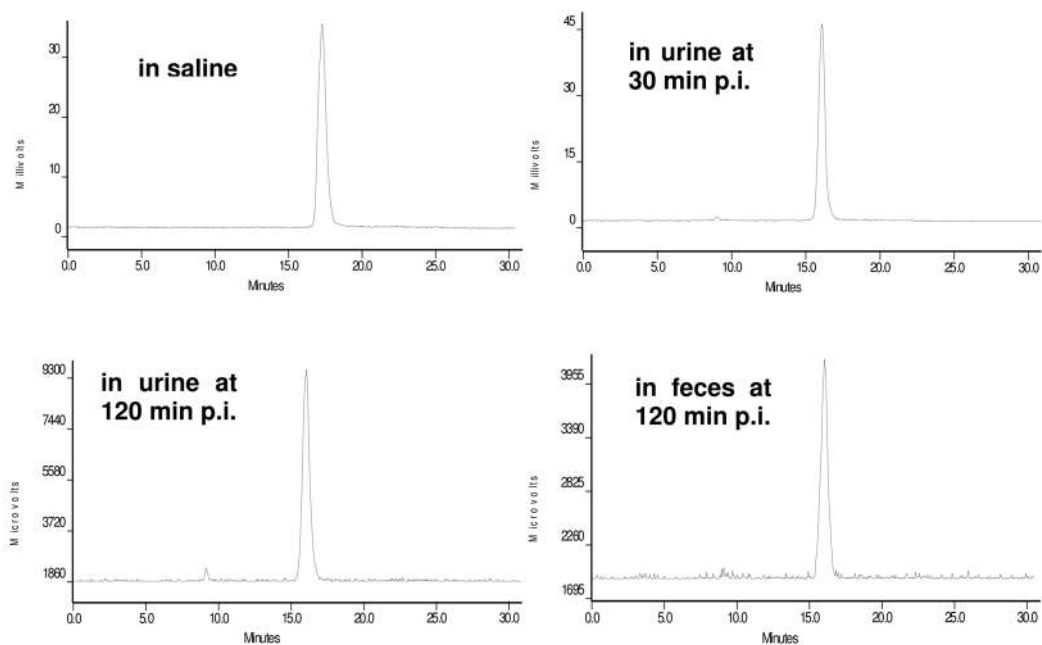
Figure 8.
Radio-HPLC chromatograms of ^{99m}Tc-2PEG$_4$-dimer in saline before injection, in urine at 30 min and 120 min p.i., and in feces at 120 min p.i. Two normal mice were used and each was administered with ~ 100 μCi of ^{99m}Tc-2PEG$_4$-dimer.
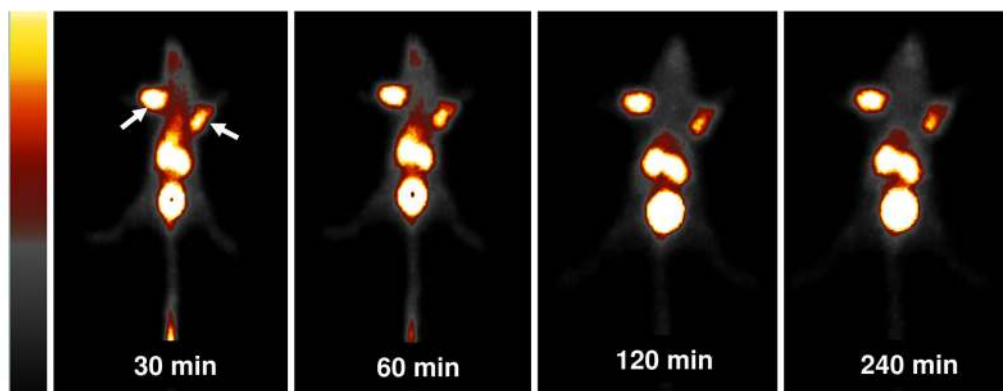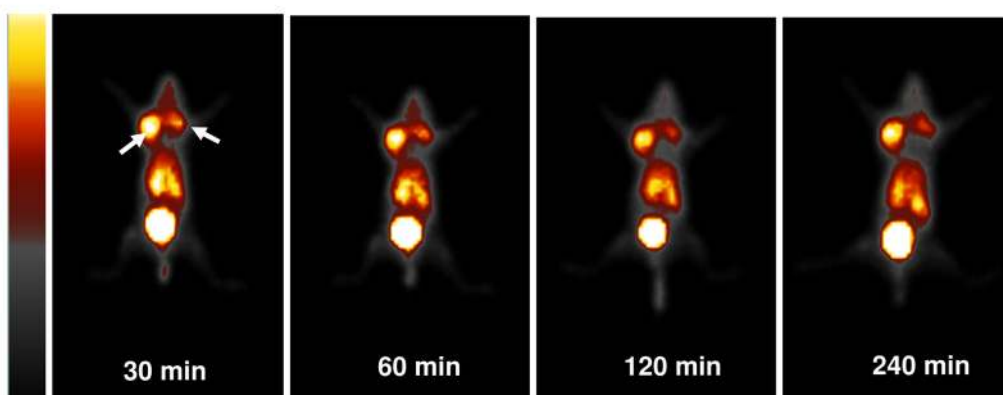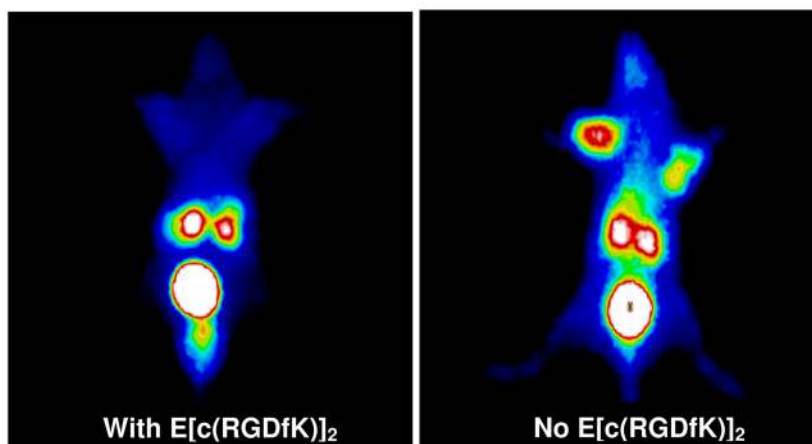
Figure 9.
Representative static images of the tumor-bearing mice (top: U87MG glioma xenografts; bottom: MDA-MB-435 breast cancer xenografts) injected with 500 – 800 μCi of ^{99m}Tc-3PEG$_4$-dimer and at 30, 60, 120 and 240 min p.i. Arrows indicate the presence of tumors.
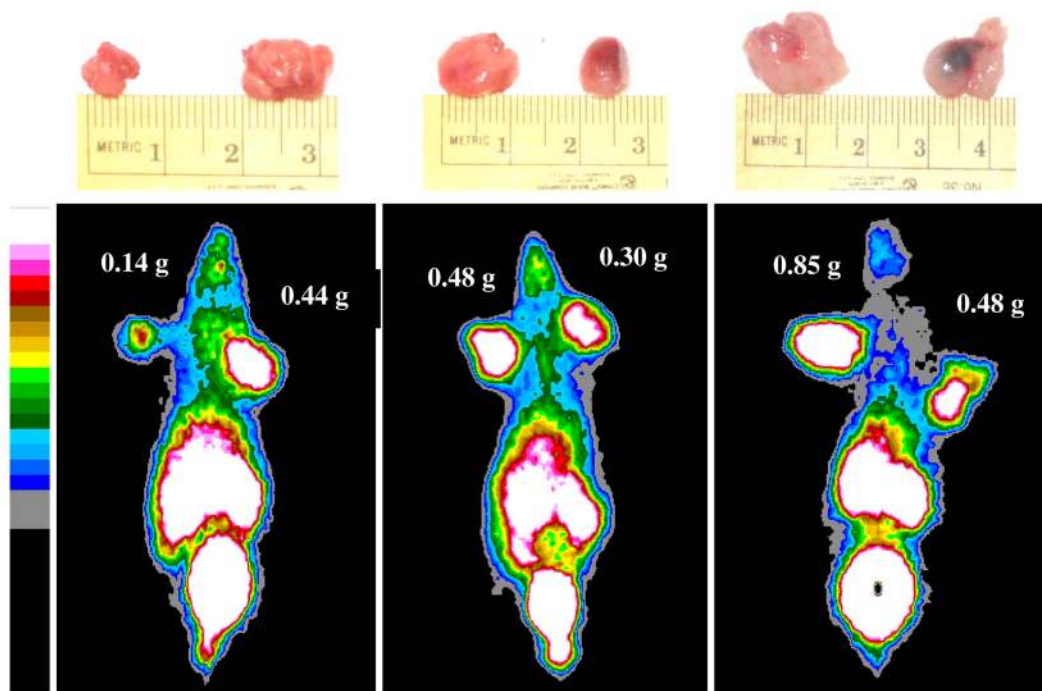
Figure 10.
Panel A: The 60 min static images of ^{99m}Tc-3PEG$_4$-dimer in the absence/presence of E[c (RGDfK)]$_2$ at 60 min p.i. to demonstrate its integrin $\alpha_v\beta_3$ specificity. Co-injection of excess E[c(RGDfK)]$_2$ resulted in significant reduction in the uptake of ^{99m}Tc-3PEG$_4$-dimer in the tumor and organs in the abdominal area. Panel B: The 60 min static images of ^{99m}Tc-3PEG$_4$-dimer in the athymic nude mice with different glioma tumor sizes (0.14 g – 0.85 g or 140 – 850 mm^3).

Table 1

HPLC retention time and log P values for ^{99m}Tc-labeled cyclic RGD peptides.

Compound	RCP (%)	Retention Time (min)	Log P Value
^{99m}Tc-PEG$_4$-monomer	> 97	8.81	−4.23 ± 0.21
^{99m}Tc-PEG$_4$-dimer	> 92	12.61	−3.56 ± 0.16
^{99m}Tc-2PEG$_4$-dimer	> 97	15.69	−4.04 ± 0.15
^{99m}Tc-3PEG$_4$-dimer	> 95	22.91	−3.96 ± 0.05